J. Fluid Mech. (1979), *vol.* 90, *part* 3, *pp.* 465–507
Printed in Great Britain

Numerical solution of wave scattering problems in the parabolic approximation

By SÉBASTIEN M. CANDEL

Office National d'Etudes et de Recherches Aérospatiales (ONERA) and
Université de Technologie de Compiègne, 92320 Châtillon, France

(Received 21 April 1978)

A numerical analysis of two-dimensional wave scattering problems is performed. The treatment relies on the parabolic approximation and provides the forward scattered wave field. Two problems are considered in particular: (i) the scattering of plane waves by a cylindrical inhomogeneity of uniform refraction index, (ii) the scattering of plane waves by a viscous core vortex. The structure of the scattered field is examined in detail and the numerical solutions of the two problems are compared to analytical results obtained in the Born approximation and interpreted according to the method of smooth perturbation.

1. Introduction

Wave scattering problems are of importance in numerous domains such as electromagnetic propagation in the earth's upper atmosphere, optical beam transmission in fibres, laser radiation, acoustic propagation in the atmosphere and under water, seismic waves in the earth's crust, free surface waves on a variable bottom etc. The present analysis is concerned with the scattering of acoustic waves by temperature and velocity inhomogeneities. It is based on the paraxial or parabolic approximation and deals with two elementary (but typical) two-dimensional problems: (i) the scattering of plane waves by a temperature (or refraction index) inhomogeneity having a cylindrical shape with a circular or elliptical cross-section, (ii) the scattering of plane waves by a viscous core vortex.

These two situations are simple but their analysis may help in comprehending more complicated practical problems encountered in acoustics such as: (i) acoustic wave propagation across the shear layer of a free jet; (ii) sound scattering by atmospheric turbulence; (iii) detection of the trailing vortices of wide body aircraft; (iv) determination of the detailed structure of a turbulent field from information contained in a scattered wave field.

The first of these problems is of particular importance in aeroacoustics. This situation is for example that of internal noise radiating from the jet engine tail pipe. It is also encountered in the anechoic open wind tunnel facilities used to simulate the forward flight effects on aircraft noise radiation.

Experimental observations performed in this type of installation by Candel, Guedel & Julienne (1975, 1976*a*, *b*, 1977) indicate that a coherent sound wave may be strongly scattered and that as a consequence acoustic measurements like spectral and cross-spectral densities coherence and sound pressure level are affected by this mechanism.

Now, a direct numerical analysis of one of these complicated situations would be

hazardous and it appears useful to first develop and check numerical tools in the case of simpler problems allowing a physical interpretation and possibly a quantitative comparison with analytical results. Indeed even the parabolic approximation which forms the basis of the present analysis is still unfamiliar and an evaluation of its possibilities is also needed.

At this point it is worth giving some details on this approximation. Mathematically, the parabolic approximation consists of replacing the equation describing the interaction between an inhomogeneous medium and an acoustic field by a parabolic equation. In this manner the propagation problem becomes a Cauchy problem and the pressure field may be calculated from its value in an initial section. Physically it consists of neglecting the waves scattered backwards by the medium and only dealing with the waves propagating in the forward direction around the incidence axis. Claerbout (1976) gives an excellent discussion and Woude & Bremmer (1975) present interesting theoretical considerations of this forward scattering approximation.

In a number of situations the scattering cross-section has reduced values for the higher scattering angles and the backscattered waves are an order of magnitude weaker than those scattered forward around the incidence direction (see for instance the measurements performed by Baerg & Schwarz (1966), theoretical results presented by Lighthill (1953); Monin (1962); Tatarski (1961, 1971) and discussions given below). These observations suggest that the backscattered waves may be neglected in many cases and that the parabolic approximation is well suited to the analysis of forward scattering problems. Indeed numerous theoretical studies of scattering by turbulence have been conducted with various types of paraxial approximations and this approach is well illustrated in two monographs by Tatarski (1961, 1971).

In optics the paraxial approximation (sometimes called the Fresnel approximation) is classically used to analyse radiation and propagation problems in free space. More recently, it has been applied in numerical calculations of laser beam propagation. One of the first studies of this subject seems to be due to Kelley (1965) and concerns the nonlinear self-focusing of optical beams. Other examples are provided by Wallace & Lilly (1974), Lilly & Miller (1977) who analyse the propagation and blooming of pulsed laser beams in the atmosphere. Ulrich (1975) gives a general review of the numerical techniques and principal results obtained in this domain.

In acoustics the parabolic approximation forms the basis of a restricted but increasing number of numerical studies of underwater propagation (Hardin & Tappert 1973; McDaniel 1975, 1976; De Santo, Perkins & Baer 1977). The scattering of sound waves by turbulent media is treated extensively but with analytical methods relying on various classical approximations such as (i) the Born approximation, (ii) the method of smooth perturbations (also called Rytov's method of smoothing), (iii) the parabolic equation method, (iv) kinetic theory and transport equations. The monographs of Tatarski (1961, 1971), the review papers presented by Barabanenkov, Kravtsov, Rytov & Tatarski (1971) and by Ishimaru (1977) describe in detail the problems, methods and principal results obtained in this research area. In addition Frisch (1968) gives an interesting discussion of the mathematical techniques applicable to the study of wave propagation in random media.

Outside the optical domain the parabolic approximation does not seem to have been widely applied to the numerical analysis of scattering problems. One objective of this study is to demonstrate its usefulness for dealing with such problems. To allow

a good comprehension of the numerical results obtained we first develop (§ 2) the parabolic equation describing the interaction of an acoustic field and a turbulent medium. A brief description of the finite difference method used for solving this equation is given in § 3. A more detailed presentation and applications to radiation problems may be found in a separate note (Candel 1977). Section 4 concerns the scattering of plane waves by a cylindrical inhomogeneity having a circular or elliptical cross-section and a uniform index of refraction. The scattering of plane sound waves by a viscous core vortex is examined in § 5. Appendices A and B provide analytical solutions of these two problems, based on the Born approximation, and appendix C recalls the relation existing between the Born approximation and the method of smooth perturbation. This relation is used in our comparison of analytical and numerical results.

2. Parabolic equation for a medium containing temperature and velocity inhomogeneities

The propagation of a weak acoustic field in a turbulent medium characterized by (i) velocity fluctuations much smaller than the sound speed ($u/c_0 \ll 1$), (ii) temperature fluctuations much smaller than the ambient temperature ($T'/T_0 \ll 1$) (iii) a low mean flow Mach number ($M_0 = u_0/c_0 \ll 1$), may be conveniently described by the following equation:

$$\nabla^2 p - \frac{1}{c_0^2}\frac{\partial^2 p}{\partial t^2} = -\frac{\partial}{\partial x_i}\left(\frac{T'}{T_0}\frac{\partial p}{\partial x_i}\right) - 2\rho_0 \frac{\partial^2 u_i v_j}{\partial x_i \partial x_j}. \tag{1}$$

In this expression T' and u_i represent the temperature and velocity fluctuations in the medium, p and v_j are the perturbations associated with the acoustic field and T_0, ρ_0, c_0 designate the mean temperature, density and sound speed. Equation (1) describes the linear interactions between the turbulent and sound fields. Various methods yield this equation or similar forms. Lighthill (1963), Howe (1973), and Ffowcs Williams & Howe (1973) start from Lighthill's equation

$$\frac{\partial^2 \rho}{\partial t^2} - c_0^2 \nabla^2 \rho = \frac{\partial^2}{\partial x_i \partial x_j} \rho u_i u_j + \nabla^2 (p - c_0^2 \rho), \tag{2}$$

written in absence and presence of the sound field. By subtracting the equations corresponding to these situations Ffowcs Williams & Howe (1973) find an equation describing the linear and nonlinear (up to second order) interactions of the medium fluctuations and acoustic perturbations.

Another method consists of starting with a development of all the field variables in sums of three terms mean flow, turbulent fluctuation, acoustic perturbation – and writing the Navier–Stokes and energy equations in the presence and absence of the exterior sound field. After subtraction of the equations obtained in these two cases, a certain amount of algebra and various order of magnitude considerations lead to (1). This approach is that of Huang (1975) who also treats the case of a finite mean flow Mach number.

Now, when the propagation medium is (or may be considered as) time independent and in the case of a monochromatic incident sound field, (1) becomes

$$\nabla^2 p + k^2 p = -\frac{\partial}{\partial x_i}\left(\frac{T'}{T_0}\frac{\partial p}{\partial x_i}\right) - 2\rho_0 \frac{\partial^2 u_i v_j}{\partial x_i \partial x_j}. \tag{3}$$

The acoustic velocity perturbations may be eliminated by making use of the linearized momentum equation, thus yielding

$$\nabla^2 p + k^2 p = -\frac{\partial}{\partial x_i}\left(\frac{T'}{T_0}\frac{\partial p}{\partial x_i}\right) - \frac{2}{i\omega}\frac{\partial^2}{\partial x_i \partial x_j}\left(u_i \frac{\partial p}{\partial x_j}\right). \tag{4}$$

If the turbulent field is assumed to be incompressible ($\partial u_i/\partial x_i = 0$) the last equation becomes

$$\begin{aligned}\nabla^2 p + k^2 p = &-\frac{\partial}{\partial x_i}\left(\frac{T'}{T_0}\right)\frac{\partial p}{\partial x_i} - \frac{T'}{T_0}\frac{\partial^2 p}{\partial x_i \partial x_i} \\ &-\frac{2}{i\omega} u_i \frac{\partial}{\partial x_i}\left(\frac{\partial^2 p}{\partial x_i \partial x_j}\right) - \frac{2}{i\omega}\frac{\partial u_i}{\partial x_j}\frac{\partial^2 p}{\partial x_i \partial x_j}.\end{aligned} \tag{5}$$

Starting from this expression we shall now develop an equation for the scattered field in the Born approximation and next derive a propagation equation based on the parabolic approximation.

Scattered field equation in the Born approximation

The Born approximation consists of replacing the field variable p by the sum of an incident (p_0) and a scattered (p_s) field, $p = p_0 + p_s$, and then of neglecting the interaction between the scattered and turbulent fluctuations. Performing these operations on (5) leads to

$$\begin{aligned}\nabla^2 p_s + k^2 p_s = &-\frac{\partial}{\partial x_i}\left(\frac{T'}{T_0}\right)\frac{\partial p_0}{\partial x_i} - \frac{T'}{T_0}\frac{\partial^2 p_0}{\partial x_i \partial x_i} \\ &-\frac{2}{i\omega} u_i \frac{\partial}{\partial x_i}\left(\frac{\partial^2 p_0}{\partial x_j \partial x_j}\right) - \frac{2}{i\omega}\left(\frac{\partial u_i}{\partial x_j}\right)\frac{\partial^2 p_0}{\partial x_i \partial x_j}.\end{aligned} \tag{6}$$

If the incident field is a plane wave

$$p_0(\mathbf{r}) = \exp(i\mathbf{k}\,.\,\mathbf{r}) = \exp(ik\mathbf{m}\,.\,\mathbf{r}), \tag{7}$$

where $\mathbf{m}$ designates a unit vector in the wave vector direction, (6) becomes

$$\nabla^2 p_s + k^2 p_s = \left[k^2 \frac{T'}{T_0} + 2k^2 \frac{\mathbf{u}\,.\,\mathbf{m}}{c_0} - ik\mathbf{m}\,.\,\nabla\frac{T'}{T_0} - 2ik\mathbf{mm} : \frac{\nabla \mathbf{u}}{c_0}\right] p_0, \tag{8}$$

and may be written more compactly as

$$\nabla^2 p_s + k^2 p_s = p_0\, 2k^2 \left(1 - \frac{i\mathbf{m}\,.\,\nabla}{k}\right)\left(\frac{1}{2}\frac{T'}{T_0} + \frac{\mathbf{m}\,.\,\mathbf{u}}{c_0}\right). \tag{9}$$

This expression is given by various authors Monin (1962), Clifford & Brown (1970), Clifford (1972), Tatarski (1971). Monin (1962) notes that

$$n' = -\left(1 - \frac{i\mathbf{m}\,.\,\nabla}{k}\right)\left(\frac{1}{2}\frac{T'}{T_0} + \frac{\mathbf{m}\,.\,\mathbf{u}}{c_0}\right) \tag{10}$$

acts like an index fluctuation for a plane wave propagating in the direction of **m**. Clifford (1972) gives an interesting physical meaning to the quantity

$$n_1 = -\left(\frac{1}{2}\frac{T'}{T_0} + \frac{\mathbf{m}.\mathbf{u}}{c_0}\right). \tag{11}$$

For this he considers the generalized index of the medium, defined as the ratio between a reference sound celerity c_0 and the local phase velocity of a plane wave propagating in the **m** direction:

$$N = \frac{c_0}{c_\phi} = \frac{c_0}{c + \mathbf{u}.\mathbf{m}}. \tag{12}$$

For weak turbulent fluctuations

$$c \simeq c_0(1 + T'/2T_0),$$

and

$$N \simeq 1/(1 + T'/2T_0 + \mathbf{u}.\mathbf{m}/c_0), \tag{13}$$

or

$$N \simeq 1 - \left(\frac{T'}{2T_0} + \frac{\mathbf{u}.\mathbf{m}}{c_0}\right) = 1 + n_1. \tag{14}$$

Thus n_1 appears as the generalized index fluctuation for a wave propagating in the **m** direction.

Thus, in the Born approximation, the scattered field satisfies an inhomogeneous Helmholtz equation (9). The right-hand side of this expression contains the index n_1 and its derivative in the incidence direction:

$$\nabla^2 p_s + k^2 p_s = -2k^2 p_0 n_1 + 2ikp_0 \mathbf{m}.\nabla n_1. \tag{15}$$

Because this equation is linear, the scattered field may be decomposed as a sum of two terms $p_s = p_s^1 + p_s^2$ which separately satisfy

$$\nabla^2 p_s^1 + k^2 p_s^1 = -2k^2 p_0 n_1, \tag{16}$$

$$\nabla^2 p_s^2 + k^2 p_s^2 = 2ikp_0 \mathbf{m}.\nabla n_1. \tag{17}$$

It is of interest to our analysis to estimate the relative magnitude of these two scattered waves. Indeed it is a simple matter to show that in the far field (the Fraunhofer region)

$$p_s^2 = \frac{\mathbf{K}.\mathbf{m}}{k} p_s^1, \tag{18}$$

where **K** denotes the 'converted' wave vector, i.e. the difference between the scattered ($k\mathbf{n}$) and incident ($k\mathbf{m}$) wave vectors

$$\mathbf{K} = k(\mathbf{n} - \mathbf{m}). \tag{19}$$

Then

$$p_s^2 = (\mathbf{m}.\mathbf{n} - 1)p_s^1, \tag{20}$$

and if Θ represents the scattered angle between directions **m** and **n**

$$|p_s^1|/|p_s^2| = 1/2\sin^2 \tfrac{1}{2}\Theta. \tag{21}$$

For scattering angles $\Theta \leqslant 30°$ this ratio is greater than 7·5 and p_s^2 is negligible compared to p_s^1.

Therefore, in the vicinity of the incidence direction the full equation (15) may be replaced by the simpler expression

$$\nabla^2 p_s + k^2 p_s = -2k^2 n_1 p_0 = 2k^2 \left(\frac{1}{2}\frac{T'}{T_0} + \frac{\mathbf{m}.\mathbf{u}}{c_0}\right) p_0. \tag{22}$$

We note that this last equation forms the basis of Tatarski's first monograph and in view of our discussion the results presented are only applicable to low scattering angle situations, i.e. to forward scattering. For higher scattering angles, the full equation (15) must be used (Kraichnan's remark in Tatarski 1961 and also Monin 1962; Tatarski 1971).

Propagation equation in the parabolic approximation

To transform (5) into a parabolic expression we write the pressure field in the form

$$p(\mathbf{r}) = p_0(\mathbf{r})\,\psi(\mathbf{r}), \tag{23}$$

where $p_0(\mathbf{r})$ represents the incident sound field such as for example a plane wave $\exp(ik\mathbf{m}.\mathbf{r})$ and $\psi(\mathbf{r})$ is an unknown function which, due to its definition, exhibits only slow variations in the incidence direction.

Upon substitution of (23) the left-hand side of (5) becomes

$$(2i\mathbf{k}.\nabla\psi + \nabla^2\psi)\exp(i\mathbf{k}.\mathbf{r}).$$

The right-hand side of (5) appears as the sum of four terms describing the linear interaction between the acoustic and turbulent fields. Consider for example

$$\frac{T'}{T_0}\frac{\partial^2 p}{\partial x_i\,\partial x_i} = \frac{T'}{T_0}\left(-k^2\psi + 2ik_i\frac{\partial\psi}{\partial x_i} + \frac{\partial^2\psi}{\partial x_i\,\partial x_i}\right)\exp(i\mathbf{k}.\mathbf{r}). \tag{24}$$

In the parabolic approximation ψ is a slowly varying function so that

$$|k^2\psi| \gg \left|2k_i\frac{\partial\psi}{\partial x_i}\right|,\ |\nabla^2\psi|. \tag{25}$$

By keeping only the leading term in (24):

$$\frac{T'}{T_0}\frac{\partial^2 p}{\partial x_i\,\partial x_i} \simeq -\frac{T'}{T_0}k^2\psi\exp(i\mathbf{k}.\mathbf{r}). \tag{26}$$

Similar simplifications may be used for the other terms of the right-hand side of (5).

This yields

$$2i\mathbf{k}.\nabla\psi + \nabla^2\psi = \left[-i\mathbf{k}.\nabla\frac{T'}{T_0} - 2ik\mathbf{mm}:\nabla\frac{\mathbf{u}}{c_0} + k^2\frac{T'}{T_0} + 2k^2\frac{\mathbf{m}.\mathbf{u}}{c_0}\right]\psi, \tag{27}$$

which may be cast in the compact form

$$2i\mathbf{k}.\nabla\psi + \nabla^2\psi = 2k^2\psi\left(1 - \frac{i\mathbf{m}.\nabla}{k}\right)\left(\frac{1}{2}\frac{T'}{T_0} + \frac{\mathbf{m}.\mathbf{u}}{c_0}\right). \tag{28}$$

We note that the interaction term looks similar to the one obtained in the Born approximation.

There is however an important difference: the index n' now multiplies the function ψ to be determined while (15) only exhibits a product of n' and the incident field p_0. The interaction term is here 'parametric'.

To cast (28) into a parabolic form it is convenient to choose one reference axis (for example Oz) parallel to the incidence direction. The parabolic approximation then consists of neglecting $\partial^2\psi/\partial z^2$ with respect to the other terms of the left-hand side:

$$|\partial^2\psi/\partial z^2| \ll |2ik\,\partial\psi/\partial z|, |\nabla_\perp^2\psi|, \tag{29}$$

and (28) becomes

$$2ik\frac{\partial\psi}{\partial z} + \nabla_\perp^2\psi = 2k^2\psi\left(1 - \frac{i}{k}\frac{\partial}{\partial z}\right)\left(\frac{1}{2}\frac{T'}{T_0} + \frac{u_z}{c_0}\right). \tag{30}$$

The following analysis is based on a simplified version of this equation obtained by neglecting

$$-2ik\psi\frac{\partial}{\partial z}\left(\frac{1}{2}\frac{T'}{T_0} + \frac{u_z}{c_0}\right). \tag{31}$$

While this simplification cannot be precisely justified we may conjecture from our discussion of the Born approximation that the contribution of this term is, in the neighbourhood of the incidence axis, small compared to that arising from

$$2k^2\psi\left(\frac{1}{2}\frac{T'}{T_0} + \frac{u_z}{c_0}\right). \tag{32}$$

As the parabolic equation is only applicable to essentially forward scattering this simplification seems consistent (but of course not essential and the whole analysis could have been carried with the full equation (30)).

Thus the numerical results presented in the following sections pertain to the reduced equation

$$2ik\frac{\partial\psi}{\partial z} + \nabla_\perp^2\psi = 2k^2\psi\left(\frac{1}{2}\frac{T'}{T_0} + \frac{u_z}{c_0}\right). \tag{33}$$

In some cases we replaced the right-hand side by a term of the form $-k^2(N^2-1)\psi$, where the refractive index N is related to the temperature or velocity fluctuations by

$$N^2 - 1 = -2\left(\frac{1}{2}\frac{T'}{T_0} + \frac{u_z}{c_0}\right) = 2n_1. \tag{34}$$

3. Numerical solution method

Various numerical methods are discussed in Candel (1977). We use here the Crank–Nicholson scheme on a double scale grid.

The parabolic equation written in two dimensions is first cast in dimensionless form using the following system of reduced co-ordinates:

$$x_* = x/L, \quad z_* = z/z_1, \tag{35}$$

where $z_1 = 4\pi L^2/\lambda$, L being a characteristic dimension of the calculation domain.

This leads to

$$i\frac{\partial\psi}{\partial z_*} + \frac{\partial^2\psi}{\partial x_*^2} + k_*^2(N^2-1)\psi = 0, \tag{36}$$

where $k_* = kL = 2\pi L/\lambda$ is a dimensionless wavenumber.

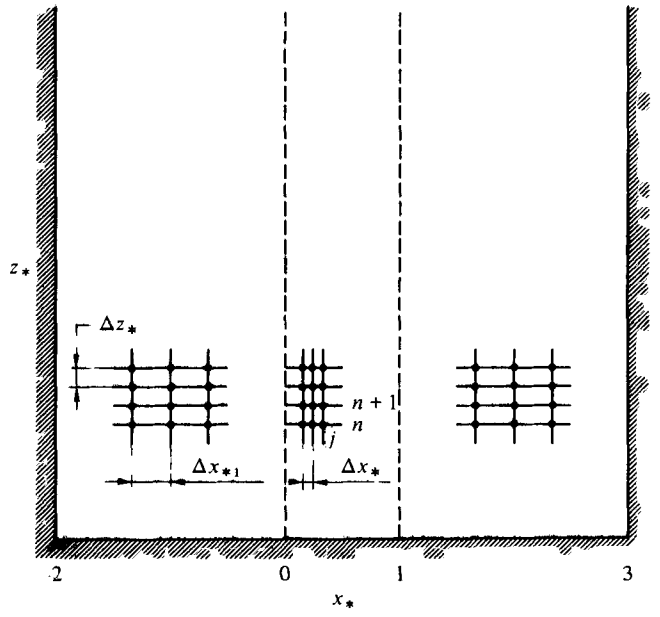

FIGURE 1. Double scale calculation grid. In the central region the nodes are separated by $\Delta x_* = 0{\cdot}005$. In the external regions $\Delta x_{1*} = 4\Delta x_* = 0{\cdot}02$. In the axial direction $\Delta z_* = 0{\cdot}0002$.

If $\psi(j\Delta x_*, n\Delta z_*) = \psi_j^n$ designates the value taken by the field variable at the nodes of the calculation grid, (36) written in finite difference form according to the Crank–Nicholson method becomes

$$-r\psi_{j+1}^{n+1} + (2 + 2r + 2q)\,\psi_j^{n+1} - r\psi_{j-1}^{n+1} = r\psi_{j+1}^n - (2r - 2)\,\psi_j^n + r\psi_{j-1}^n, \tag{37}$$

where $$r = i\Delta z_*/(\Delta x_*)^2,$$

and $$q = ik_*^2(N^2 - 1)\,\Delta z_*.$$

In writing this expression we have somewhat arbitrarily evaluated the inhomogeneous interaction term $k^2(N^2 - 1)\,\psi$ at step $n + 1$. At each step in the z direction the solution may be obtained by solving the system of equations (37) for all internal nodes ($1 < j < M$). Two additional equations are provided by the conditions set on the left and right boundaries. The system thus defined is tridiagonal and its solution may be calculated with great accuracy and speed by applying classical recursion techniques.

Now, it is shown by Candel (1977), that the solution of free space radiation problems is greatly improved if the calculation is conducted on a variable scale grid. This comes from the fact that one must impose certain boundary conditions on the limits of the domain of integration but that one cannot impose the exact conditions for a radiating field.

We therefore use (figure 1) small computation cells in the central region allowing a precise calculation of the sound field and a looser grid in the two external regions. This artificially extends the integration domain in the transverse direction without increasing the number of nodes (i.e. without increasing the computation time). All the calculations presented are performed accordingly on a grid having 401 nodes in the transverse direction. The central region ($0 \leqslant x_* \leqslant 1$) is divided in 200 intervals

$\Delta x_* = 0{\cdot}005$ while each external region ($-2 \leqslant x_* < 0$, $1 < x_* \leqslant 3$) contains 100 nodes separated by $\Delta x_{1*} = 4\Delta x_* = 0{\cdot}02$. The step size in the axial direction is in all cases $\Delta z_* = 0{\cdot}0002$.

4. Scattering by a cylindrical refraction index inhomogeneity

We here consider the scattering of a plane wave by a cylindrical inhomogeneity with a circular cross-section. In the inhomogeneous region the refraction index is uniform and in the exterior region it takes a unit value. The incident plane wave propagates in the z direction and has a unit amplitude (figure 2*a*):

$$p_0(\mathbf{r}) = \exp(i\mathbf{k}.\mathbf{r}) = \exp(ikz),$$

$$\mathbf{k} = k\mathbf{m} = (\omega/c_0)\mathbf{m}.$$

To guide our discussion of the numerical results obtained with the PEM we first present the solution of the problem derived with the help of the Born approximation.

Solution based on the Born approximation

A straightforward application of the Born approximation yields the following expression for the scattered field (while the problem is classical a simple derivation is given for completeness in appendix A):

$$p_s(\mathbf{r}) = (kR)^2 \left(\frac{\pi}{2kr}\right)^{\frac{1}{2}} [\exp(\tfrac{1}{4}i\pi + ikr)](N^2-1)\frac{J_1(KR)}{KR}. \tag{38}$$

In this expression J_1 represents the Bessel function of order 1, R is the radius of the cylindrical inhomogeneity, $K = k|\mathbf{n}-\mathbf{m}|$ denotes the modulus of the converted wave vector while $\mathbf{n}$ and $\mathbf{m}$ are respectively unit vectors in the observation and incidence direction. The converted wave vector modulus appears very generally in scattering problems. Its value is classically expressed in terms of the scattering angle Θ formed by the incident and scattered direction:

$$K = k[n^2 + m^2 - 2\mathbf{n}.\mathbf{m}]^{\frac{1}{2}} = 2k|\sin\tfrac{1}{2}\Theta|. \tag{39}$$

At a given observation point $\mathbf{r}$, the total acoustic field is the sum of the incident plane wave and the scattered wave (38):

$$p(\mathbf{r}) = p_0(\mathbf{r}) + p_s(\mathbf{r}). \tag{40}$$

The field appears as a superposition of a plane wave directed along the z axis and a cylindrical wave whose amplitude depends on the observation direction. The inhomogeneity acts like an induced source radiating a spatially inhomogeneous cylindrical wave. As the numerical results are expressed in terms of modulus and phase it is here worth calculating these quantities. This may be done by writing (40) in the form

$$p(\mathbf{r}) = p_0(\mathbf{r})[1 + p_s(\mathbf{r})/p_0(\mathbf{r})]. \tag{41}$$

The field modulus is then given by

$$A = \left\{\left[1 + \mathrm{Re}\left(\frac{p_s}{p_0}\right)\right]^2 + \left[\mathrm{Im}\left(\frac{p_s}{p_0}\right)\right]^2\right\}^{\frac{1}{2}}, \tag{42}$$

and the phase relative to the incident wave may be obtained from

$$\phi = \tan^{-1} \frac{\mathrm{Im}\,(p_s/p_0)}{1+\mathrm{Re}\,(p_s/p_0)}. \tag{43}$$

When the scattered wave has a small amplitude ($|p_s/p_0| \ll 1$) the preceding formulas may be approximated by

$$A \simeq 1+\mathrm{Re}\,(p_s/p_0), \tag{44}$$

$$\phi \simeq \mathrm{Im}\,(p_s/p_0). \tag{45}$$

The first of these expressions may be rearranged in a slightly different form:

$$\chi = \ln A/A_0 = \mathrm{Re}\,(p_s/p_0), \tag{46}$$

with $A_0 = 1$ designating the incident wave amplitude.

In fact, when the Born approximation solution is interpreted according to (45) and (46) it becomes identical to the solution one would obtain by applying the method of smooth perturbation (MSP) to first order. This identity is not always stated clearly in theoretical studies of scattering and we therefore give a brief proof in appendix C.

It is generally accepted (but the matter is still controversial) that the first-order smooth perturbation solution is more uniformly valid than the first-order Born approximation. For this reason we consistently adopt (45) and (46) to interpret the Born approximation solution.

Now, if a_s designates the scattered field 'amplitude',

$$a_s = (kR)^2 \left(\frac{\pi}{2kr}\right)^{\frac{1}{2}} (N^2-1)\frac{J_1(KR)}{KR}, \tag{47}$$

the field logarithmic amplitude χ and the phase ϕ are given by

$$\chi(\mathbf{r}) = a_s(\mathbf{r})\cos(\tfrac{1}{4}\pi + kr - \mathbf{k}\,.\,\mathbf{r}), \tag{48}$$

$$\phi(\mathbf{r}) = a_s(\mathbf{r})\sin(\tfrac{1}{4}\pi + kr - \mathbf{k}\,.\,\mathbf{r}). \tag{49}$$

These two expressions indicate that the sound field oscillates in amplitude and phase. This behaviour, associated to the spatial variations of

$$\tfrac{1}{4}\pi + kr - \mathbf{k}\,.\,\mathbf{r} = \tfrac{1}{4}\pi + k(x^2+z^2)^{\frac{1}{2}} - kz, \tag{50}$$

is a direct result of the interference between the incident plane sound wave and the scattered cylindrical wave. As the scattered field amplitude $a_s(r)$ is spatially modulated by the function $J_1(KR)/KR$, the magnitude of the interference fringes, at a constant radius r, changes with the observation angle:

$$\frac{a_s(r,\Theta)}{a_s(r,0)} = \frac{2J_1(KR)}{KR} = \frac{2J_1(2kR|\sin\tfrac{1}{2}\Theta|)}{2kR|\sin\tfrac{1}{2}\Theta|}. \tag{51}$$

One may note in particular that the backscattered amplitude becomes small when the product kR is superior to $\sim 1{\cdot}5$:

$$\frac{a_s(r,\pi)}{a_s(r,0)} = \frac{2J_1(2kR)}{2kR}.$$

If for example $R = \frac{1}{2}\lambda$ ($kR = \pi$) the preceding ratio is about $-0{\cdot}06$. Indeed, it is generally observed that the backscattered field becomes weaker when the ratio R/λ of a characteristic dimension of the scatterer to the wavelength increases. Now, the

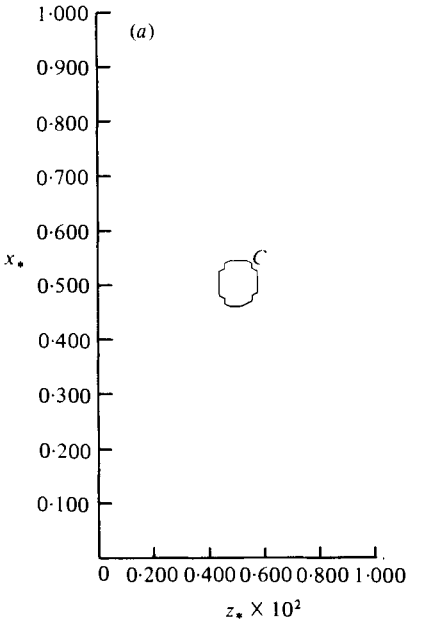

FIGURE 2(*a*). For legend see page 477.

parabolic approximation is based on the assumption that the backscattered waves may be neglected in comparison to the forward scattered waves (this point is well explained by Claerbout 1976). In the two situations analysed with the PEM, the ratio $a_s(r, \pi)/a_s(r, 0)$ is about 0·18 ($R = \frac{1}{4}\lambda$) and $-0{\cdot}06$ ($R = \frac{1}{2}\lambda$) and we cannot positively state that the parabolic approximation is fully justified. Nevertheless the results obtained appear qualitatively correct and they come close to the MSP solution. In fact, limitations of the PEM are not well defined and we intend to give in the future a detailed numerical analysis of this aspect. Returning to (48) and (49) we note that further evidence of the interference phenomenon may be obtained by examining the transverse structure of the pressure field.

For this analysis it is convenient and consistent with the parabolic approximation to suppose that $|x/z| \ll 1$. Equations (48) and (49) thus become

$$\phi(x, z) = a_s(x, z) \sin\left(\tfrac{1}{4}\pi + \frac{kx^2}{2z}\right), \tag{52}$$

$$\chi(x, z) = a_s(x, z) \cos\left(\tfrac{1}{4}\pi + \frac{kx^2}{2z}\right). \tag{53}$$

The logarithmic amplitude and phase appear as amplitude-modulated Fresnel gratings.

On the z axis

$$\phi(0, z) = a_s(0, z)/2^{\frac{1}{2}}, \tag{54}$$

$$\chi(0, z) = a_s(0, z)/2^{\frac{1}{2}}.$$

When the observation point leaves the axis the phase begins to increase and goes through a first maximum when

$$Fr = \frac{kx^2}{2z} \simeq \tfrac{1}{4}\pi. \tag{55}$$

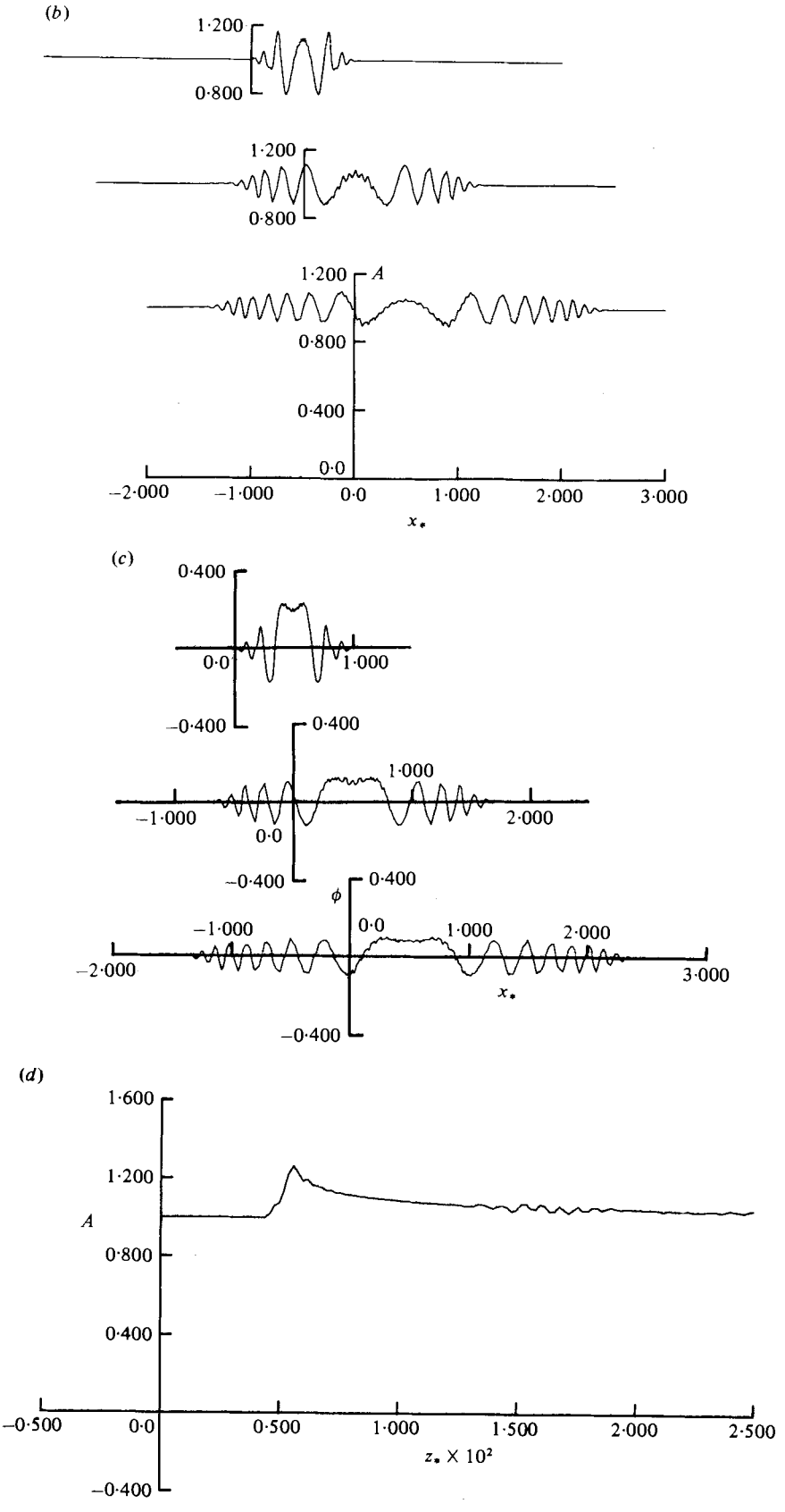

FIGURES 2 (*b*, *c*, *d*). For legend see page 477.

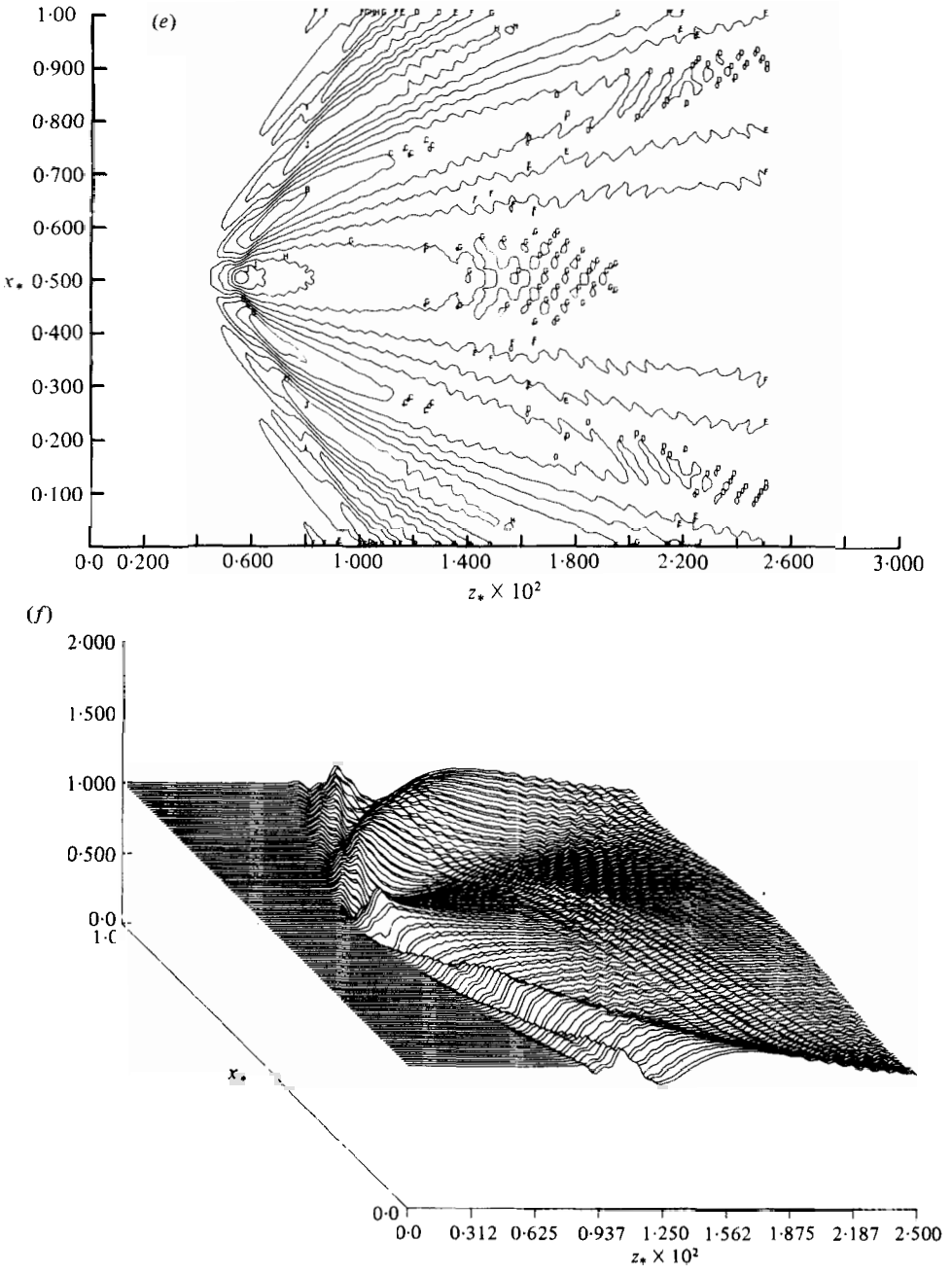

FIGURE 2. Scattering of a plane wave by a cylindrical inhomogeneity of uniform index $N = 1{\cdot}2$. The cylinder has a circular cross-section of radius $R_* = 0{\cdot}0389$ and is centred at $x_{c*} = 0{\cdot}5$, $z_{c*} = 0{\cdot}005$. The incident wave propagates in the positive z direction with a wavelength $\lambda_* = 4R_*$. (*a*) Geometry of the problem. (In the reduced system of co-ordinates the circular cross-section appears slightly distorted.) (*b*) Field modulus in three axial sections $\bar{z}_* = 0{\cdot}003$, $0{\cdot}011$, $0{\cdot}109$. (*c*) Phase calculated with respect to the incident wave and represented in three axial sections $\bar{z}_* = 0{\cdot}003$, $0{\cdot}011$, $0{\cdot}019$. (*d*) Variation of the field modulus on the $x_* = 0{\cdot}5$ axis. (*e*) Iso-contour plot of the field modulus, $A = 0{\cdot}74$, $B = 0{\cdot}79$, $C = 0{\cdot}85$, $D = 0{\cdot}90$, $E = 0{\cdot}95$, $F = 1{\cdot}00$, $G = 1{\cdot}06$, $H = 1{\cdot}11$, $I = 1{\cdot}16$, $J = 1{\cdot}21$, $K = 1{\cdot}27$. (*f*) Field modulus in perspective.

The logarithmic amplitude decreases and exhibits its first minimum for

$$Fr = \frac{kx^2}{2z} \simeq \tfrac{3}{4}\pi. \tag{56}$$

We are now ready to present the numerical results obtained with the PEM.

Numerical solution of the parabolic equation

Figures 2(*b*)–(*f*) present the results obtained by solving the parabolic equation with the finite difference method of § 3. The plots are all given in reduced co-ordinates ($x_* = x/L$, $z_* = z/z_1$, $z_1 = 4\pi L^2/\lambda$) and may be scaled to real dimensions by choosing an appropriate value for L. To conserve the greatest degree of generality to the numerical algorithm the origin of co-ordinates does not coincide with the centre of the inhomogeneity. We designate by x_{c*} and z_{c*} the co-ordinates of the centre and by $\bar{x}_* = x_* - x_{c*}$ and $\bar{z}_* = z_* - z_{c*}$ co-ordinates measured with respect to this point.

In this first example, we have selected an inhomogeneity having a radius

$$R_* = R/L = 0{\cdot}0389$$

centred at $x_{c*} = 0{\cdot}5$, $z_{c*} = 0{\cdot}005$, an index of refraction $N = 1{\cdot}2$ and a wavelength $\lambda = 4R$ ($\lambda_* = 0{\cdot}1556$).

Figure 2(*b*) shows the field modulus in three axial sections situated at $\bar{z}_* = 0{\cdot}003$, $0{\cdot}011$, $0{\cdot}019$.

The field modulus appears as expected in the form of a Fresnel grating. The predicted decrease in the neighbourhood of the axis may also be noticed but one finds that

$$(\chi)_{\text{axis}}/(\chi)_{\text{first maximum}} \simeq 0{\cdot}55, \tag{57}$$

which significantly differs from the MSP value of $\sim 2^{-\frac{1}{2}}$.

If we now consider the position of the first two minima we note that, for $\bar{z}_* = 0{\cdot}019$, $\bar{x}_* = 0{\cdot}42$ and the corresponding Fresnel number

$$Fr = \frac{(k(\bar{x}))^2}{2\bar{z}} = \frac{\bar{x}_*^2}{4\bar{z}_*} \simeq 2{\cdot}32$$

takes a value which is close to but different from that ($\frac{3}{4}\pi$) obtained for the Born approximation solution. However, replacing the $\frac{1}{4}\pi$ phase shift of (53) by $\phi_0 = 0{\cdot}26\pi$ we obtain a good approximation for the pressure field modulus in a form very similar to (53):

$$\chi = \ln A/A_0 = \hat{a}_\chi(\bar{x}_*, \bar{z}_*) \cos\left[\phi_0 + (\bar{x}_*)^2/4\bar{z}_*\right]. \tag{58}$$

Here $\hat{a}_\chi(\bar{x}_*, \bar{z}_*)$ designates the envelope of the Fresnel grating plotted on a logarithmic scale.

The field phase (figure 2*c*) also appears as a Fresnel grating.

After an initial increase from the axis it reaches its first two maxima at $|\bar{x}_*| = 0{\cdot}23$ when $\bar{z}_* = 0{\cdot}019$. The corresponding Fresnel number $Fr = (\bar{x}_*)^2/4\bar{z}_* \simeq 0{\cdot}696$ differs slightly from the predicted value of $\frac{1}{4}\pi$. By replacing the $\frac{1}{4}\pi$ phase shift of expression (52) by $\phi_0 = 0{\cdot}34$ it is possible to represent the phase by

$$\phi(x_*, z_*) = \hat{a}_\phi(x_*, z_*) \sin\left[\phi_0 + (\bar{x}_*)^2/4\bar{z}_*\right]. \tag{59}$$

To complete this discussion it is of interest to compare the maximum values of the amplitude functions a_s (Born approximation), $\hat{a}_\chi$ and $\hat{a}_\phi$ (parabolic equation method).

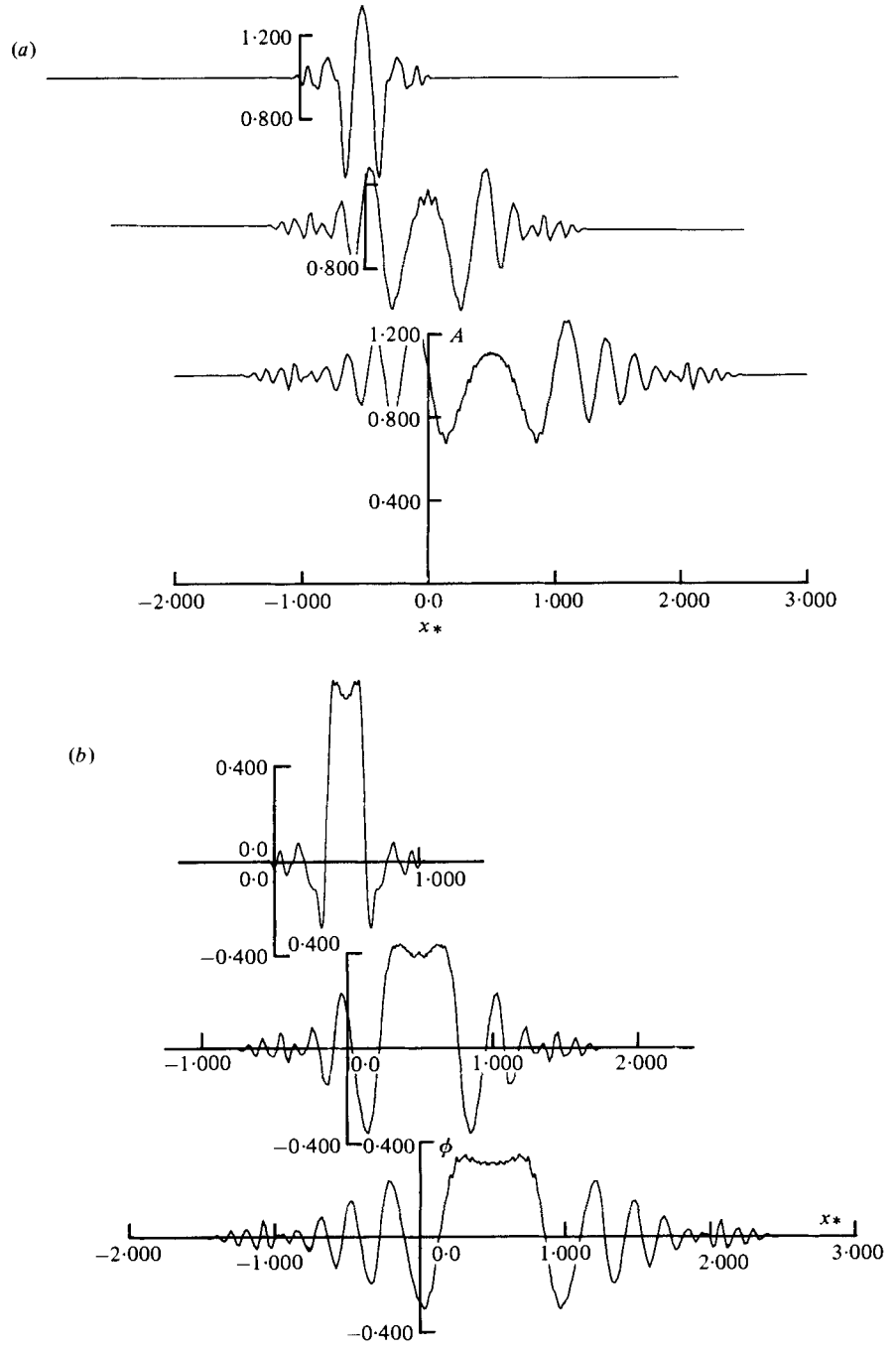

FIGURES 3(*a*, *b*). For legend see page 481.

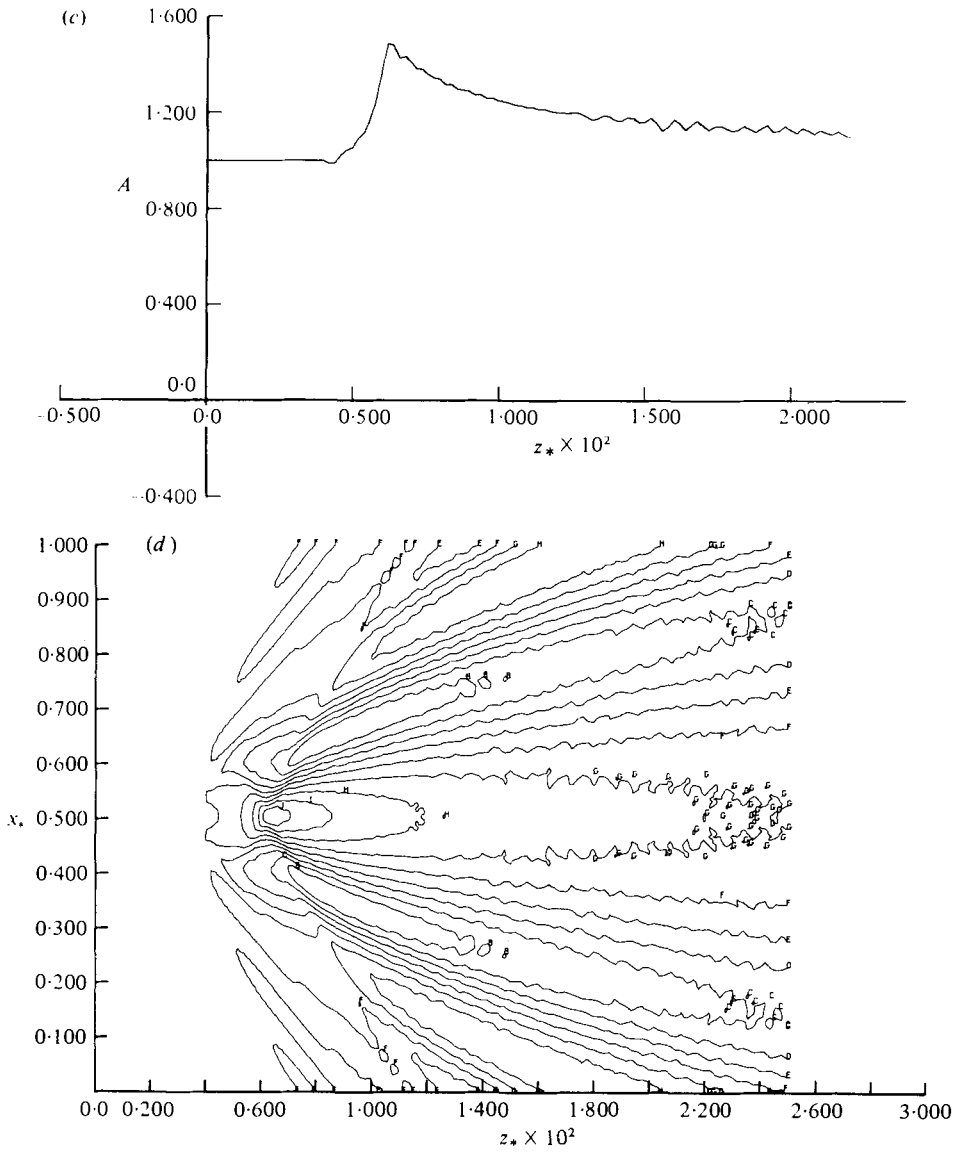

FIGURES 3(*c*, *d*). For legend see page 481.

Table 1 gives the values of these three quantities for the three sections of figures 2(*b*) and (*c*). We note that $\hat{a}_\chi$ and $\hat{a}_\phi$ deduced from the parabolic equation solution are very nearly equal and that their values are strikingly close to that of a_s. Of course, this comparison is not performed between an exact solution and a numerical solution but between two kinds of approximations. However the agreement obtained is significant in view of the fact that these two approximations are substantially different.

Further information on the nature of the scattered field may be obtained by considering its variation in the axial direction. One finds from the field modulus of figure 2(*d*) that the logarithmic amplitude $(\ln A/A_0)$ tends to zero like $(\bar{z}_*)^{-\frac{1}{2}}$, which is typical of a cylindrical wave. Figures 2(*e*) and 2(*f*) give a more complete description

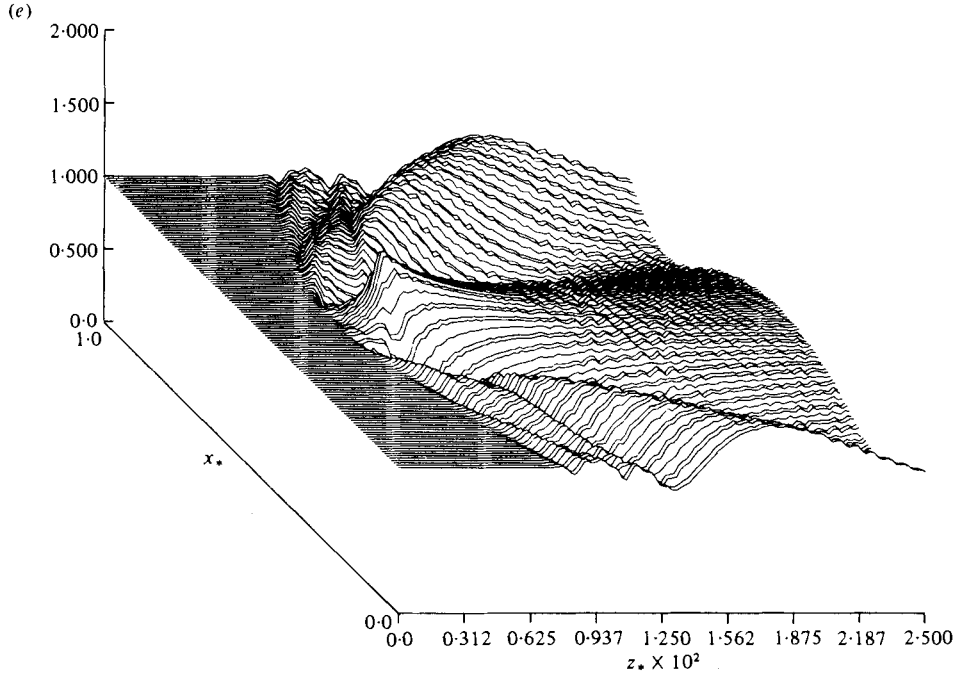

FIGURE 3. Scattering of a plane wave by a cylindrical inhomogeneity of uniform index $N = 1{\cdot}2$. The cylinder has a circular cross-section of radius $R_* = 0{\cdot}0789$ and is centred at $x_{c*} = 0{\cdot}5$, $z_{c*} = 0{\cdot}005$. The incident wave propagates in the positive z direction with a wavelength $\lambda_* = 2R_*$. (*a*) Field modulus in three axial sections $\bar{z}_* = 0{\cdot}003$, $0{\cdot}011$, $0{\cdot}019$. (*b*) Phase calculated with respect to the incident wave and represented in three axial sections $\bar{z}_* = 0{\cdot}003$, $0{\cdot}011$, $0{\cdot}019$. (*c*) Variation of the field modulus on the $x_* = 0{\cdot}5$ axis. (*d*) Iso-contour plot of the field modulus, $A = 0{\cdot}49$, $B = 0{\cdot}59$, $C = 0{\cdot}69$, $D = 0{\cdot}79$, $E = 0{\cdot}90$, $F = 1{\cdot}00$, $G = 1{\cdot}10$, $H = 1{\cdot}20$, $I = 1{\cdot}30$, $J = 1{\cdot}41$, $K = 1{\cdot}51$. (*e*) Field modulus in perspective.

	MSP	PEM	
$\bar{z}_*$	Max a_s	Max $\hat{a}_\chi$	Max $\hat{a}_\phi$
0·003	0·221	0·229	0·228
0·011	0·116	0·115	0·126
0·019	0·088	0·100	0·098

TABLE 1. Comparison between the maximum 'amplitude' functions obtained with the method of smooth perturbations and the parabolic equation method.

of the pressure field. The modulus is plotted in the central region $0 \leqslant x_* \leqslant 1$ in the form of iso-contours and in perspective.

The two figures clearly show the fringes produced by the interference of the incident and scattered waves. The ridges and troughs are located along constant Fresnel number parabolas

$$Fr = \frac{k(\bar{x})^2}{2\bar{z}} = \frac{(\bar{x}_*)^2}{4\bar{z}_*} = \text{constant}. \tag{60}$$

	MSP	PEM	
$\bar{z}_*$	a_s	Max $\hat{a}_\chi$	Max $\hat{a}_\phi$
0·003	0·885	0·65	0·82
0·011	0·462	0·471	0·455
0·019	0·352	0·361	0·353

TABLE 2. Comparison between the maximum 'amplitude' functions obtained with the method of smooth perturbations and the parabolic equation method.

A second set of figures 3(*a–e*) gives some indications on the effect of a change in the characteristic scale to wavelength ratio. For this case, the wavelength has been kept constant while the radius has been doubled

$$(R_* = R/L = 0{\cdot}0779, \quad \lambda_* = 2R_*, \quad k_* = 2\pi R/\lambda = \pi).$$

The same general remarks apply in this case; however the phase shift ϕ_0 which must be used to represent the logarithmic amplitude and phase in the forms (52) and (53) is of the order of $0{\cdot}46\pi$ and thus differs markedly from the $\frac{1}{4}\pi$ value given by the MSP. The maximum amplitudes a_s, $\hat{a}_\chi$ and $\hat{a}_\phi$ are comparable except at a short distance from the scatterer (table 2). These amplitudes are about four times as large as those of the previous case, corresponding to a $(kR)^2$ dependence of the scattered field. The general structure of the fringe pattern remains unchanged in the dimensionless co-ordinates x_*, z_* as can be seen by comparing figures 2(*e*) and 3(*d*) or 2(*f*) and 3(*e*).

Scattering by a cylindrical inhomogeneity of elliptical cross-section

We here extend the foregoing analysis to a slightly different geometry. Our objective is essentially illustrative but we also intend to describe briefly the transition between the 'geometric' near field of the scatterer and the diffraction-dominated far field.

The inhomogeneity is a cylinder of elliptical section defined by

$$1 = (x_* - x_{c*})^2/a_*^2 + (z_* - z_{c*})^2/b_*^2 = (\bar{x}_*)^2/a_*^2 + (\bar{z}_*)^2/b_*^2. \tag{61}$$

Figures 4(*a–h*) present the results obtained for $a_* = 0{\cdot}04$, $b_* = 0{\cdot}158$ and an incident wavelength equal to the longitudinal semi-axis $\lambda_* = b_* = 0{\cdot}158$. The modulus and phase of the field plotted on figures 4(*a*) and (*b*) for six transverse sections $\bar{z}_* = -0{\cdot}001$, 0·003, 0·007, 0·011, 0·015 and 0·019 appear with the now familiar Fresnel grating structure. On the central axis $x_* = 0{\cdot}5$ the modulus tends asymptotically to one like $(\bar{z}_*)^{-\frac{1}{2}}$ (figure 4*c*) and the fringe pattern of figures 4(*d*) and (*e*) has the parabolic structure already observed on figures 2(*e*, *f*) and 3(*d*, *e*).

Figure 4(*f*) indicates the position of a sequence of wave fronts separated by a phase interval of $0{\cdot}225 \times 2\pi$. In the region occupied by the elliptical scatterer the wave fronts progress more slowly as the sound celerity is – in the case treated here – inferior to that of the ambient medium:

$$\Delta c/c_0 = (c - c_0)/c_0 = 1/N - 1 \simeq -0{\cdot}167.$$

The region where the wave fronts are retarded is not geometrically limited to the inhomogeneous region; it overlaps the edges of the scatterer and sees its transverse

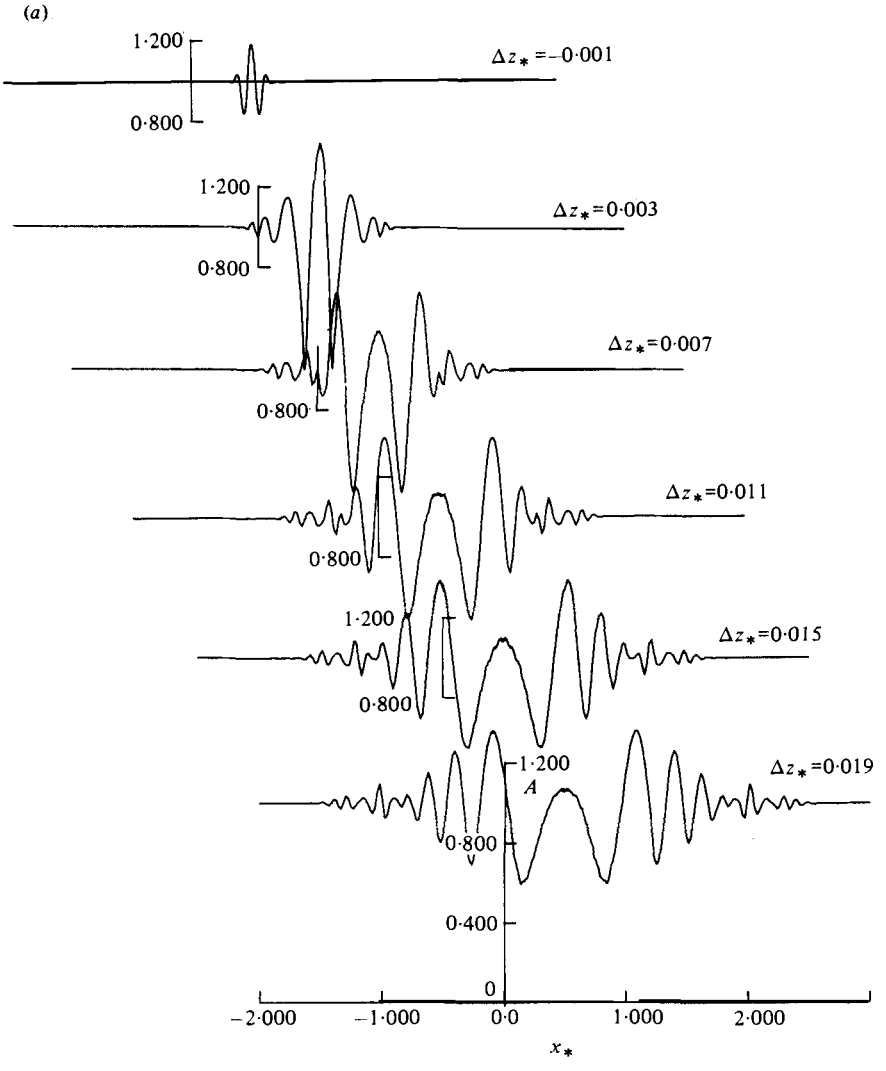

FIGURE 4(*a*). For legend see page 487.

dimension increase like $(\bar{z}_*)^{\frac{1}{2}}$ with a simultaneous decrease in the phase variation. This behaviour notably departs from that which one would expect from a purely geometric description of propagation.

Wave diffraction very rapidly dominates the refraction effects and the pressure field exhibits a geometrical character only in the immediate vicinity of the scatterer (on figures 4*a* and *b* for $\bar{z}_* = -0{\cdot}001$ and still perceptible for $\bar{z}_* = 0{\cdot}003$).

Finally figures 4(*g*) and (*h*) are presented as *a posteriori* justifications of the validity of the numerical integration. They give a view of the complete calculation domain ($-2 \leqslant x_* \leqslant 3$) with the 'external' regions plotted with a scale four times smaller than in the central region. Even at the largest axial distance $z_* = 0{\cdot}025$ the scattered field exhibits a very small amplitude on the left and right limits and the wavefronts are very nearly perpendicular to the axial direction. As a consequence the Neumann

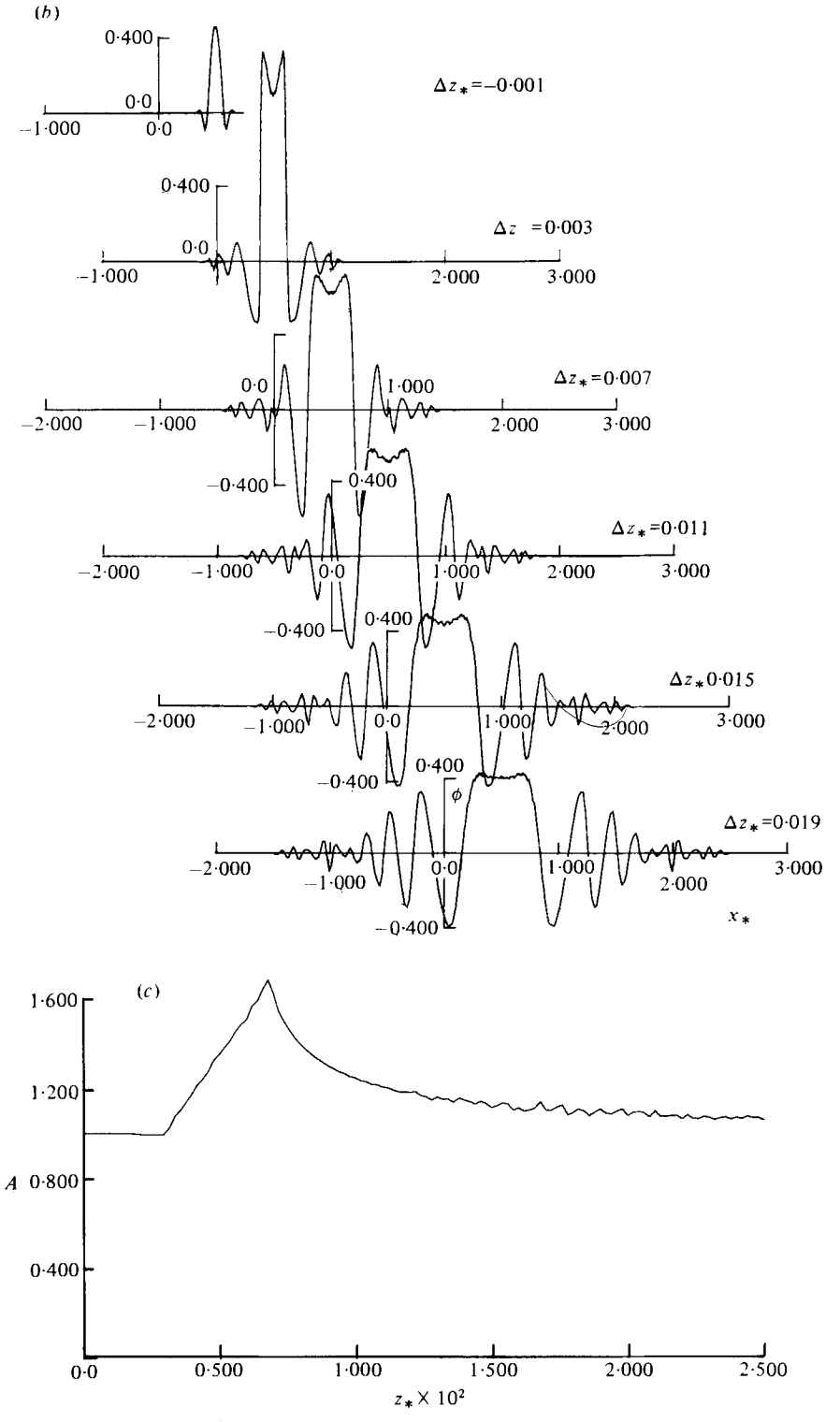

FIGURES 4(*b*, *c*). For legend see page 487.

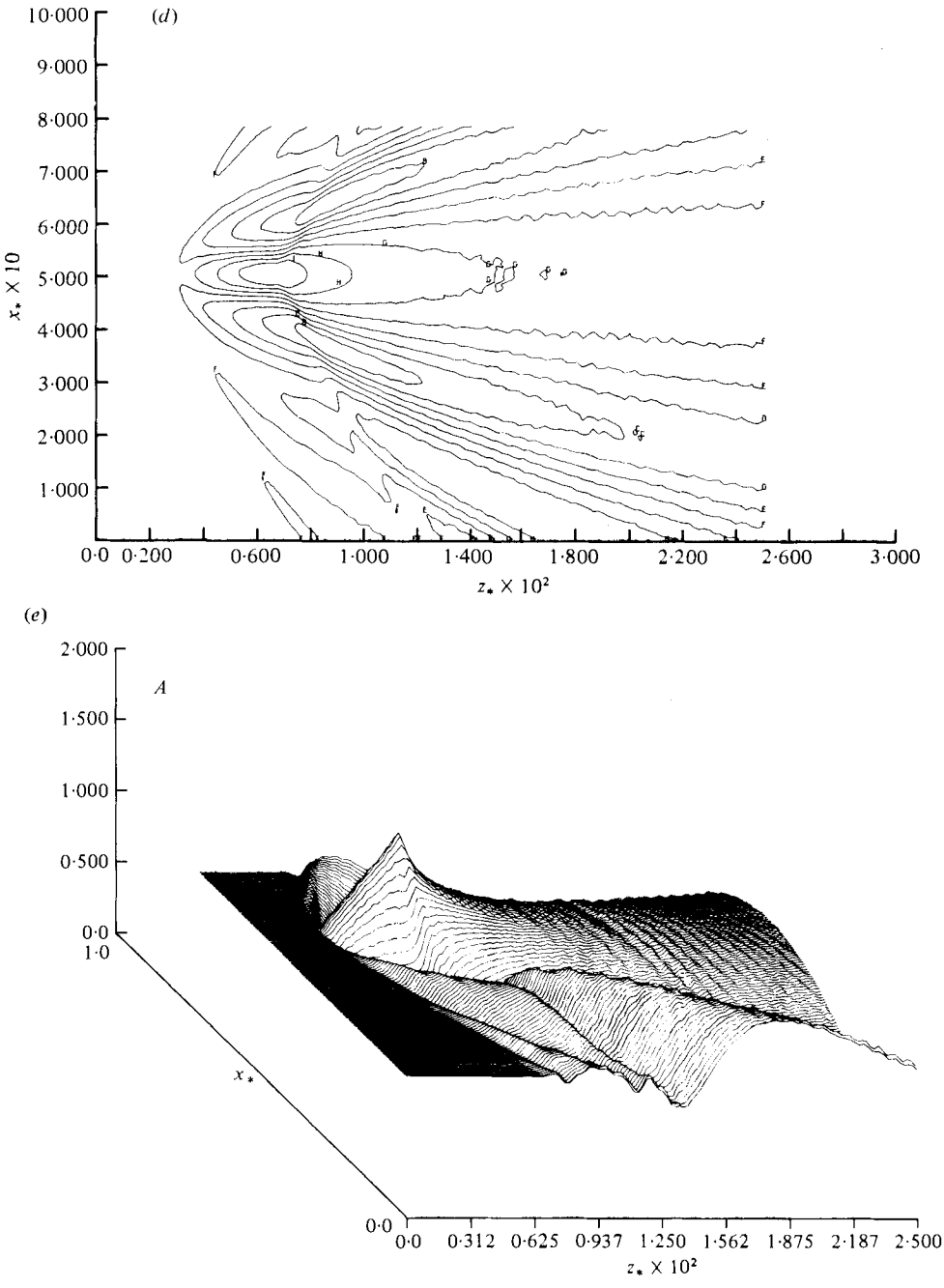

FIGURES 4(*d*, *e*). For legend see page 487.

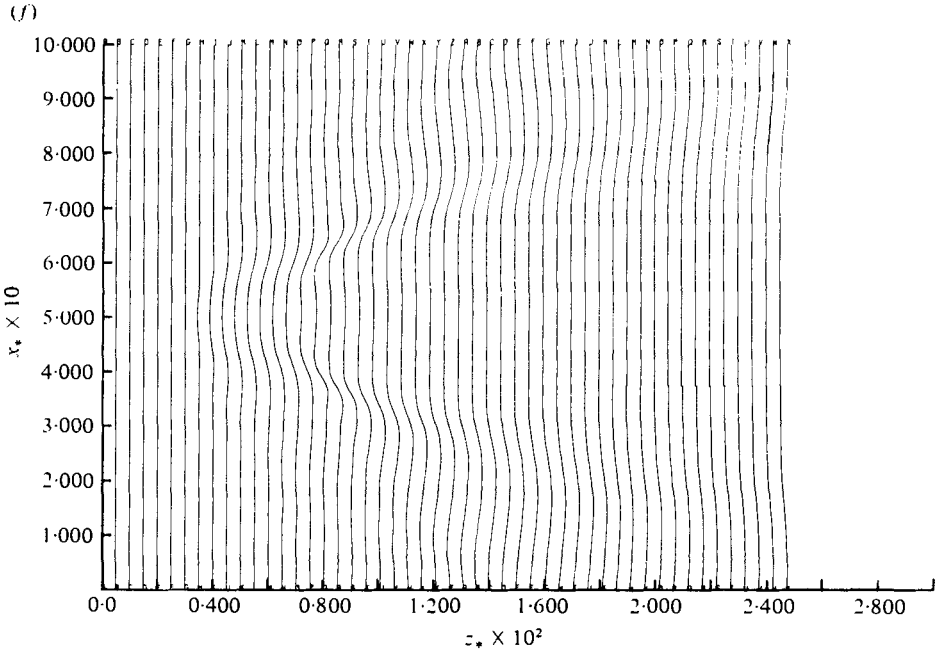

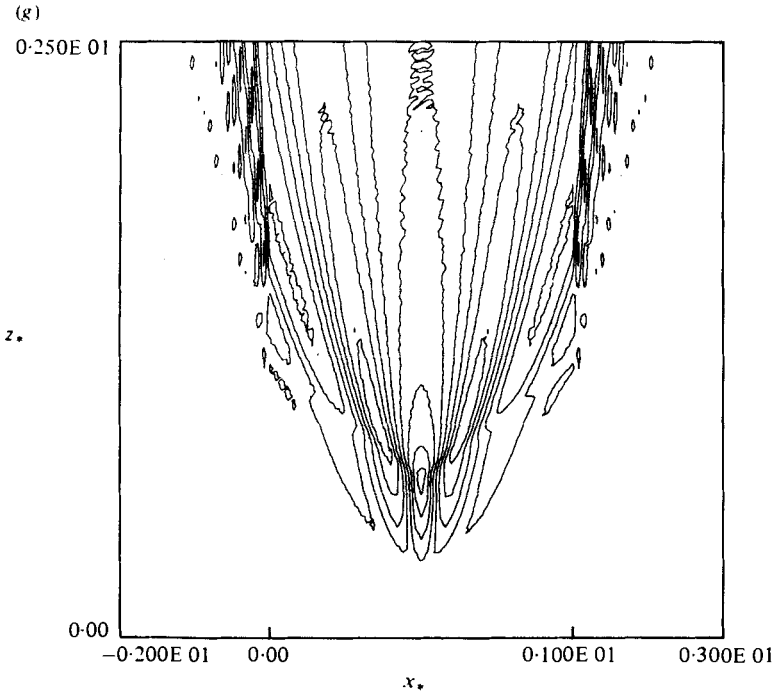

FIGURES 4 (*f*, *g*). For legend see page 487.

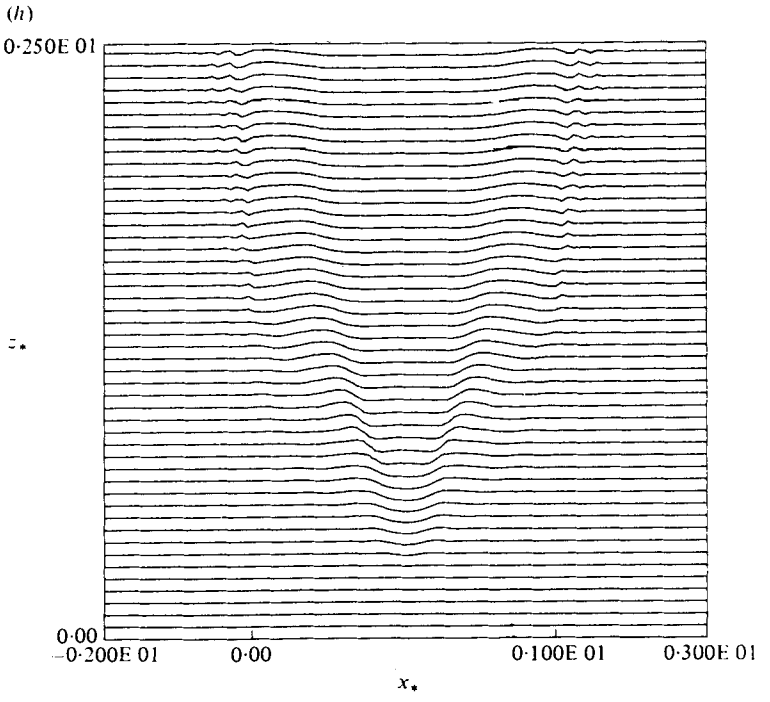

FIGURE 4. Scattering of a plane wave by a cylindrical inhomogeneity of uniform index $N = 1{\cdot}2$. The cylinder has an elliptical cross-section defined by $(\bar{x}_*)^2/a_*^2 + (\bar{z}_*)^2/b_*^2 = 1$, $a_* = 0{\cdot}04$, $b_* = 0{\cdot}158$ and is centred at $x_{c*} = 0{\cdot}5$, $z_{c*} = 0{\cdot}005$. The incident wave propagates in the positive z direction with a wavelength $\lambda_* = b_*$. (*a*) Field modulus in six axial sections $\bar{z}_* = -0{\cdot}001$, $0{\cdot}003$, $0{\cdot}007$, $0{\cdot}011$, $0{\cdot}015$, $0{\cdot}019$. (*b*) Phase calculated with respect to the incident wave in six axial sections $\bar{z}_* = -0{\cdot}001$, $0{\cdot}003$, $0{\cdot}007$, $0{\cdot}011$, $0{\cdot}015$, $0{\cdot}019$. (*c*) Variation of the field modulus on the $x_* = 0{\cdot}5$ axis. (*d*) Iso-contour plot of the field modulus $A = 0{\cdot}27$, $B = 0{\cdot}41$, $C = 0{\cdot}55$, $D = 0{\cdot}70$, $E = 0{\cdot}84$, $F = 0{\cdot}98$, $G = 1{\cdot}13$, $H = 1{\cdot}27$, $I = 1{\cdot}41$, $J = 1{\cdot}56$, $K = 1{\cdot}70$. (*e*) Field modulus in perspective. (*f*) Wave fronts. The phase of the first front is zero. It is $12{\cdot}5 \times 2\pi$ for the last. (*g*) Another iso-contour plot of the field modulus. The complete calculation domain is represented. In the central region ($0 < x_* < 1$) the scale is four times that used in the external regions ($-2 \leqslant x_* < 0$, $1 < x_* \leqslant 3$). (*h*) Wave fronts plotted in the whole calculation domain. The scaling is similar to that of figure 4 (*g*).

conditions imposed on the ψ function on the limits of the calculation grid have no sensible influence on the field computation.

5. Scattering of a plane wave by a viscous core vortex

This section presents an analysis of the scattering of a plane acoustic wave by a viscous core vortex (also called self-similar vortex). This elementary problem constitutes a good prototype model for the scattering of waves by large-scale velocity inhomogeneities of the kind encountered in turbulent shear flows. From a technological point of view the problem considered in this section will provide a qualitative picture of the scattering of sound waves crossing a turbulent mixing layer like that of an open wind tunnel. Recent experiments (for example, Brown & Roshko 1974; Roshko 1976; Winant & Browand 1974; Lau & Fisher 1975) indicate that turbulent mixing layers

contain an orderly vortex structure partially coherent and quasi-periodic in space and time. Other experiments (Candel *et al.* 1975, 1976*a*, *b*, 1977; Candel, Julienne & Julliand 1976) show that this large-scale coherent structure dominates the scattering process. Indeed the large-scale structure gives to the scattered field its convective, projective and wave-like nature.† It is also responsible for the formation of two distinct sidebands in the sound field spectrum. In fact the scattered field appears like a projected image of the large-scale organized motion existing in the mixing layer. In view of this evidence it seems possible to analyse the scattering of sound waves by a shear layer as a sequence of discrete events quasi-periodic in time having a spatial structure similar to that produced by the interaction of an incident wave and an isolated vortex. In proposing this description we abandon the classical approach of the problem of scattering by turbulent motion which is based on a statistical characterization of the phenomenon (typical analyses of this kind are presented by Tatarski 1961).

Now, a complete description of the scattering by a turbulent mixing layer requires detailed information on the large-scale vortices forming the coherent structure. This information is not at present complete so that we prefer using a viscous core vortex as a model for the real vortices (this choice is suggested by Legendre 1968).

Independently of this problem, another application motivates our analysis. It is the remote detection and ranging of the trailing vortices of the large transport aircraft. The persistence of these vortices in the vicinity of airports may be a cause of accidents for small business aircraft. Among the detection methods put forward, those based on the scattering of sound waves by the vortices seem promising. Most of the location systems using this principle operate in a frequency band of a few kHz and in a bistatic mode with separated transmitter and receiver. This configuration is preferable to a monostatic arrangement because the backscattering cross-section for velocity fluctuations is in principle nul or most probably very small. The analysis presented in this section corresponds to the bistatic situation for scattering angles $|\Theta| \lesssim 35°$. This limitation is that generally accepted for the parabolic equation method. For higher scattering angles the analysis could be carried in two steps: (i) use the parabolic equation to calculate the propagation of the incident wave and its interaction with the vortex; (ii) choose a new propagation direction towards the observation point and apply the parabolic equation to calculate the scattered field around this axis, the field determined in the first step providing the new initial conditions.

We shall not carry out this procedure here and shall limit our analysis to the forward scattering problem.

It is now worth reviewing the previous studies of this problem. High frequency geometrical techniques based on ray tracings are used by George (1972); Butler, Holbeche & Fethney (1973); Dowdling (1975); Candel (1976). Such analyses make evident the refractive properties of the vortex flow but they do not take account of diffraction effects and fail in the proximity of caustics which inevitably form in the neighbourhood of the vortex core. The calculation of the field in such regions requires special techniques and it is generally not performed except for very slow vortex motions and only before the caustic has formed. Low-frequency analyses based on

† In addition these experiments and in particular the correlation and coherence analysis performed between the turbulent and scattered field indicate that the scattered wave detected at a microphone is emitted when a large-scale vortex crosses the source microphone line.

the Born approximation have been performed by other authors. Muller & Matschat (1959) consider the interaction between a cylindrical vortex and a plane acoustic wave. The vortex core in their study is in solid body rotation and presents an arbitrary inclination. Ferziger (1974) considers a plane wave propagating perpendicular to a viscous core vortex. The same situation, together with the case of a cylindrical incident wave, is studied by O'Shea (1975) in a detailed manner. These three investigations based on the Born approximation lead, in the case of an infinite vortex flow, to a singular solution in the incidence direction. The singularity of the forward scattered field is associated according to O'Shea (1975) to the fact that the interaction region between the incident wave and the vortex is infinite and that the tangential velocity decreases asymptotically like r^{-1}. In this situation the Born approximation is not strictly applicable. It is generally accepted only when the wavelength is much larger than a characteristic dimension of the scatterer or more precisely when

$$(N^2-1)(kR)^2 \ll 1.$$

Nevertheless the Born approximation will help us in interpreting the results of the parabolic approximation. We intend to show that the PEM is in this problem (and in other problems of acoustic wave propagation in moving media) far superior to the more classical geometrical and low-frequency approximations.

Solution based on the Born approximation

The tangential velocity in a viscous core (self-similar) vortex is at a distance r from the axis

$$u_\theta(r) = \frac{\Gamma}{2\pi r}(1-\exp(-r^2/R^2)), \tag{62}$$

where Γ represents the circulation at a large distance from the vortex axis and R designates a characteristic scale of the flow ($R = 4\nu t$ for a viscous flow).

Another representation is sometimes convenient:

$$u_\theta(r) = \frac{\alpha u_M}{(r/R_M)}[1-\exp(-\beta(r/R_M)^2)], \tag{63}$$

where R_M 'the vortex radius' is the distance from the axis at which the tangential velocity attains its maximum value u_M. This is so if $\beta = 1{\cdot}26$ and $\alpha = 1{\cdot}40$. Equations (62) and (63) are identical if

$$\Gamma = 2\pi\alpha u_M R_M, \tag{64}$$

$$R = R_M/\beta^{\frac{1}{2}}. \tag{65}$$

We use (62) for the theoretical calculations and (63) for the numerical simulations. The Born approximation solution is derived in appendix B by techniques similar to those of Ferziger (1974) and O'Shea (1975). The result differs slightly but significantly from those given earlier.

In the case of a plane incident wave of the form $\exp(-i\omega t)$, the field scattered by the vortex is written

$$p_s(r,\Theta) = \frac{1}{(2\pi kr)^{\frac{1}{2}}}\frac{\Gamma k}{c_0}\exp(-\tfrac{1}{4}K^2R^2)[\tfrac{1}{2}\cot\tfrac{1}{2}\Theta - \sin\tfrac{1}{2}\Theta\cos\tfrac{1}{2}\Theta]\exp(ikr-\tfrac{1}{4}i\pi), \tag{66}$$

where $K = 2k\sin\frac{1}{2}\Theta$ the converted wave vector modulus appears in the exponential term only. The scattered field is the sum of two scattered waves

$$p_s(\mathbf{r}) = p_s^1(\mathbf{r}) + p_s^2(\mathbf{r}), \tag{67}$$

where

$$p_s^1(\mathbf{r}) = \frac{1}{(2\pi kr)^{\frac{1}{2}}}\frac{\Gamma k}{c_0}\exp(-\tfrac{1}{4}K^2R^2)\,\tfrac{1}{2}\cot\tfrac{1}{2}\Theta\exp(ikr - \tfrac{1}{4}i\pi), \tag{68}$$

$$p_s^2(\mathbf{r}) = -\frac{1}{(2\pi kr)^{\frac{1}{2}}}\frac{\Gamma k}{c_0}\exp(-\tfrac{1}{4}K^2R^2)\sin\tfrac{1}{2}\Theta\cos\tfrac{1}{2}\Theta\exp(ikr - \tfrac{1}{4}i\pi). \tag{69}$$

If we return to the basic interaction equation (9) written for $T'/T_0 = 0$:

$$\nabla^2 p_s + k^2 p_s = 2k^2\frac{u_z}{c_0}p_0 - \frac{2ik}{c_0}\frac{\partial u_z}{\partial z}p_0,$$

the scattered fields p_s^1 and p_s^2 correspond to the factors appearing in the right-hand side of this equation. The ratio of these two waves is

$$|p_s^1|/|p_s^2| = 1/2\sin^2\tfrac{1}{2}\Theta, \tag{70}$$

which, for small scattering angles, is sufficiently large so that p_s^2 may be neglected with respect to p_s^1. This conclusion was already reached in § 2 and on the basis of this argument we also justified the simplification of the parabolic equation (30).

Now the total field around the direction of incidence takes the form

$$p(\mathbf{r}) = p_0(\mathbf{r}) + p_s^1(\mathbf{r}) = p_0(\mathbf{r})\,(1 + p_s^1/p_0). \tag{71}$$

If this expression is interpreted according to

$$\chi = \ln A/A_0 = \mathrm{Re}\,(p_s^1/p_0), \tag{72}$$

$$\phi = \mathrm{Im}\,(p_s^1/p_0), \tag{73}$$

it identifies to the solution of the problem which would be obtained with the method of smooth perturbations to first order. Then

$$\chi = a_s\cos(\tfrac{1}{4}\pi + kr - kz)\,\mathrm{sgn}\,(\Theta\Gamma), \tag{74}$$

$$\phi = a_s\mathrm{in}\,(\tfrac{1}{4}\pi + kr - kz)\,\mathrm{sgn}\,(\Theta\Gamma), \tag{75}$$

where

$$a_s = \frac{1}{(2\pi kr)^{\frac{1}{2}}}\frac{|\Gamma|k}{c_0}\exp(-\tfrac{1}{4}K^2R^2)\,\tfrac{1}{2}|\cot\tfrac{1}{2}\Theta|, \tag{76}$$

and sgn $(\Theta\Gamma)$ is the sign of the product $\Theta\Gamma$. When the vortex induces a positive circulation ($\Gamma > 0$) expressions (74) and (75) show that, near the axis and for a positive scattering angle Θ, the logarithmic amplitude and the phase are both positive. In this case according to the definition of χ, A is superior to A_0. When the scattering angle is negative so are χ and ϕ and $A < A_0$.

One also notes that χ and ϕ are antisymmetric functions of Θ and that near the axis (in the region where the parabolic equation solution is indeed valid)

$$\chi = a_s\cos\left(\tfrac{1}{4}\pi + \frac{kx^2}{2z}\right)\mathrm{sgn}\,(\Theta\Gamma), \tag{77}$$

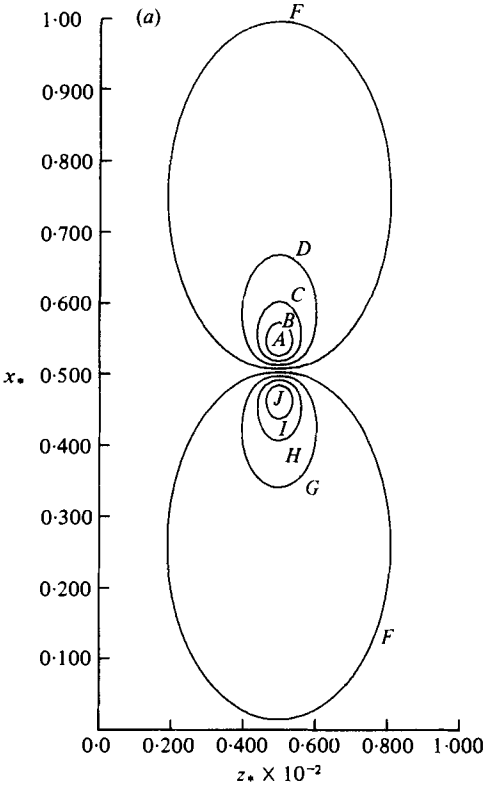

FIGURE 5(*a*). For legend see page 495.

and

$$\phi \simeq a_s \sin\left(\tfrac{1}{4}\pi + \frac{kx^2}{2z}\right) \operatorname{sgn}(\Theta\Gamma), \tag{78}$$

appear as antisymmetrical Fresnel gratings. This structure is associated with the interference between the incident plane wave and the cylindrical scattered wave. The fringes produced at a constant distance from the vortex axis are spatially modulated by the function

$$\exp(-\tfrac{1}{4}K^2R^2)|\cot\tfrac{1}{2}\Theta| = \exp(-k^2R^2\sin^2\tfrac{1}{2}\Theta|\cot\tfrac{1}{2}\Theta|, \tag{79}$$

and their amplitude decreases as the scattering angle increases.

Solution based on the parabolic equation method

Figures 5(*a–g*) display the numerical results obtained in analysing the scattering by a viscous core vortex having a radius $R_{M*} = R_M/L = 0{\cdot}0389$, a maximum tangential velocity $u_M = 20\,\mathrm{m/s}$ for an incident wavelength $\lambda = 4R_M$ ($k_* = kR_M = \frac{1}{2}\pi$). The vortex centred at $x_{c*} = 0{\cdot}5$, $z_{c*} = 0{\cdot}005$ induces a positive circulation in the propagation medium (a rotation from the x_* to the z_* axis). The motion is represented on figure 5(*a*) using the equivalent index of refraction $N^2 = 1 - 2u_z/c_0$ defined at the end of § 2. This index is smaller than one in the region where the axial velocity u_z is positive ($x_* > 0{\cdot}5$). In this half-plane the phase velocity is higher than the reference

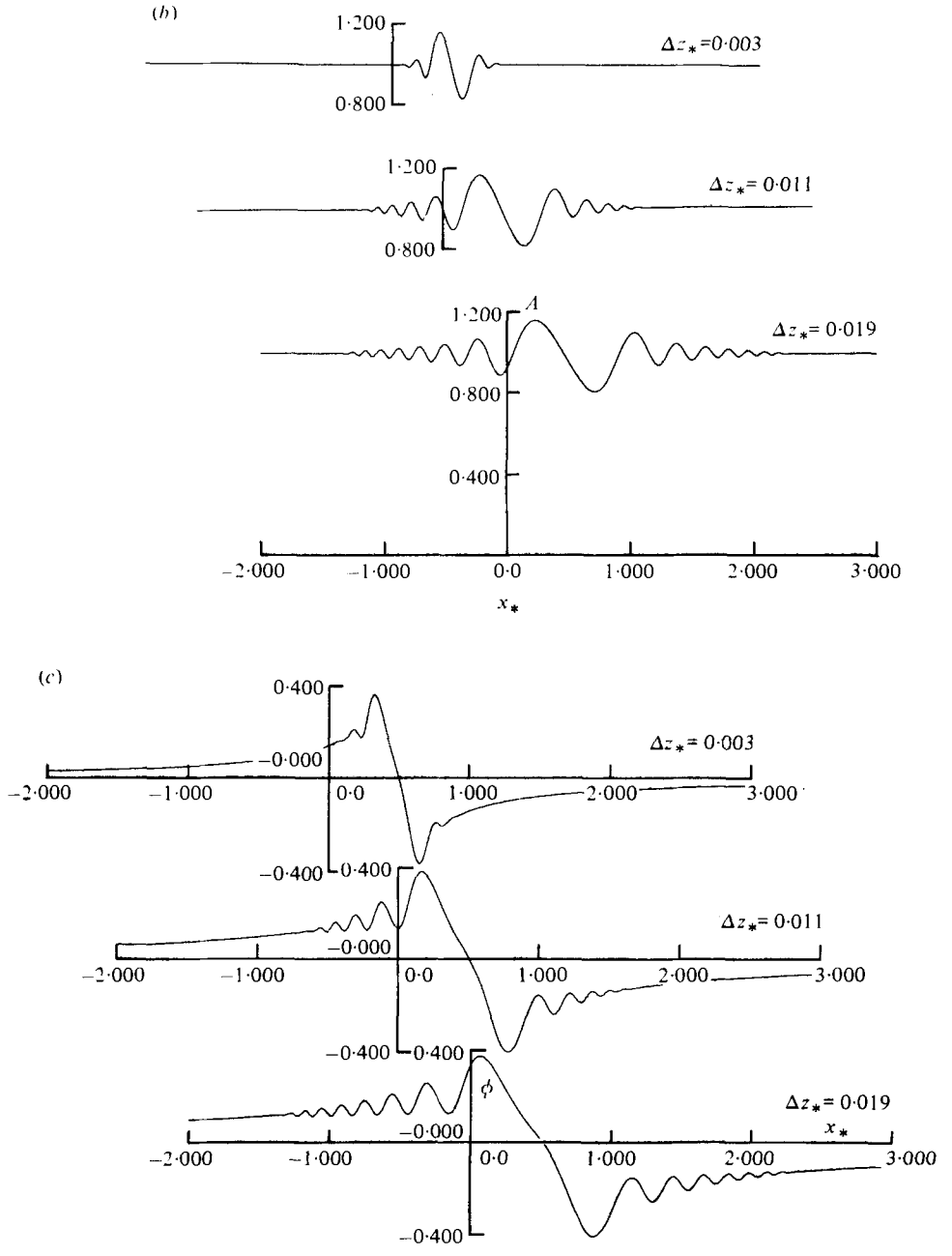

FIGURES 5(*b*, *c*). For legend see page 495.

velocity c_0 due to convection by the medium. In the other half plane ($x_* < 0{\cdot}5$) the wavefronts are retarded by the backward flow they encounter and the refraction index is greater than one. The modulus and phase of the pressure field are represented on figure 5(*b*) in three axial sections $\bar{z}_* = 0{\cdot}003$, 0·011 and 0·019. For a positive scattering angle ($x_* < 0{\cdot}5$) the modulus and phase begin by increasing from the $x_* = 0{\cdot}5$ axis; they are seen to decrease for a small negative scattering angle ($x_* > 0{\cdot}5$).

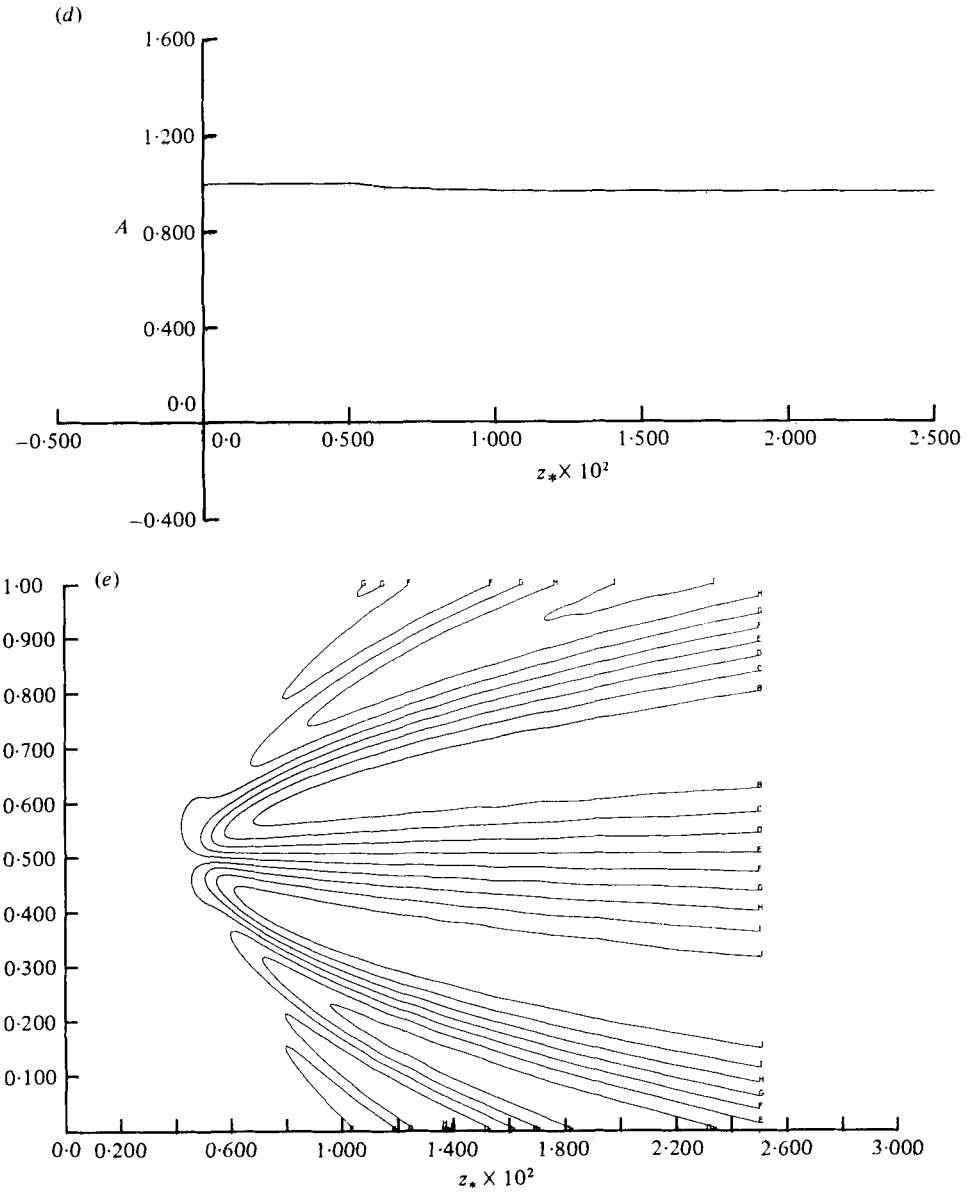

FIGURES 5 (*d*, *e*). For legend see page 495.

The modulus and phase exhibit oscillations of decreasing amplitude as the distance to the $x_* = 0{\cdot}5$ axis increases. The logarithmic amplitude

$$\chi = \ln A/A_0 \simeq (A - A_0)/A_0,$$

appears to be approximately antisymmetric. The phase is also roughly antisymmetric. The previous observations agree with those deduced from the Born approximation solution. However there are important differences. First of all the numerical solution is not singular in the axial direction. In addition, and this applies in particular to the phase, one notes that the oscillations corresponding to the fringes formed in the

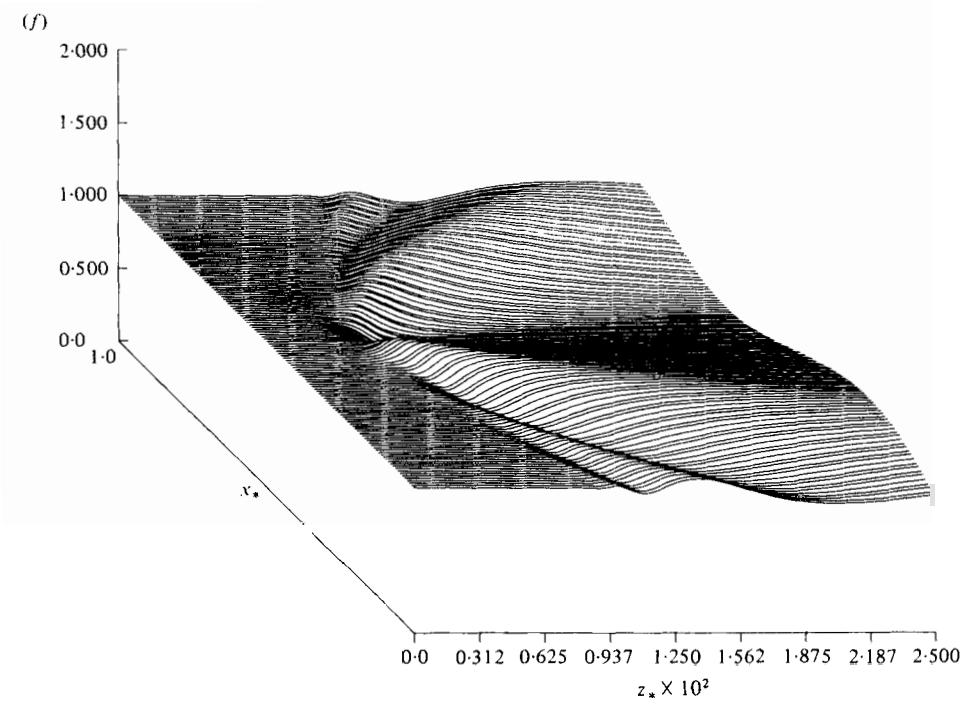

FIGURE 5(*f*). For legend see page 495.

interference of the incident and scattered fields are superposed to a mean variation of the phase or amplitude functions. The mean phase variation is associated to refraction of the sound waves in their propagation through the vortex flow: when $x_* > 0{\cdot}5$ the axial velocity u_z is positive, the waves are convected by the flow and a negative phase variation results. The inverse effect is observed in the other half-plane $x_* < 0{\cdot}5$, where the axial velocity is negative. The parabolic equation thus accounts simultaneously for the refraction and diffraction effects, demonstrating that the PEM is far superior to the low-frequency Born approximation or high-frequency geometrical approximation. The total field is thus determined by a competition between refractive and diffractive effects and it may be conjectured that, for a constant r/λ ratio and a vortex core radius R_M much smaller than the wavelength, diffraction is the dominant mechanism and produces oscillations of χ and ϕ of a kind similar to those of (77) and (78). When R_M/λ increases, refraction induces larger mean variations and the total field presents interference fringes superposed to mean amplitude and phase modulations.

Figure 5(*d*) confirms the regular behaviour of the field modulus on the central axis ($x_* = 0{\cdot}5$). The modulus decreases very slightly with distance. This may be interpreted in terms of ray acoustics by observing that the initial ray tube corresponding to the incident plane wave expands very slightly in the central region where the axial velocity is near zero. Figures 5(*e*) and (*f*) give a more complete description of the field modulus in the central region ($0 < x_* \leqslant 1$). These two figures show the central fringes and portions of the following ripples and clearly indicate the antisymmetric nature of the modulus.

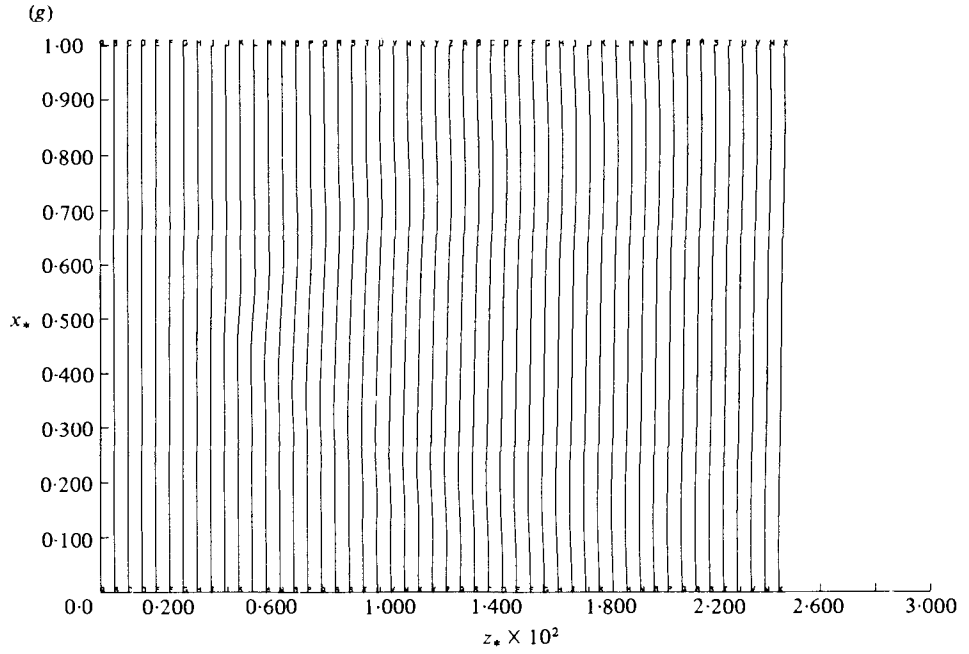

FIGURE 5. Scattering of a plane wave by a viscous core vortex. The vortex is centred at $x_{c*} = 0{\cdot}5$, $z_{c*} = 0{\cdot}005$. The tangential velocity reaches its maximum $u_M = 20\,\mathrm{m/s}$ at a distance $R_{M*} = 0{\cdot}0389$. The medium rotates in the positive direction (from the x to the z axis). The incident wave propagates in the z direction with $\lambda = 4R_M$. (*a*) Effective index $N = (1 - 2u_z/c_0)^{\frac{1}{2}}$ plotted in iso-contour form $A = 0{\cdot}941, B = 0{\cdot}954, C = 0{\cdot}967, D = 0{\cdot}980, E = 0{\cdot}993, F = 1{\cdot}006, G = 1{\cdot}019, H = 1{\cdot}032, I = 1{\cdot}045, J = 1{\cdot}058$. (*b*) Field modulus in three axial sections $\bar{z}_* = 0{\cdot}003$, $0{\cdot}011$, $0{\cdot}019$. (*c*) Phase calculated with respect to the incident wave in three axial sections $\bar{z}_* = 0{\cdot}003$, $0{\cdot}011$, $0{\cdot}019$. (*d*) Variation of the field modulus on the $x_* = 0{\cdot}5$ axis. (*e*) Iso-contour plot of the field modulus $A = 0{\cdot}81, B = 0{\cdot}84, C = 0{\cdot}88, D = 0{\cdot}92, E = 0{\cdot}95, F = 0{\cdot}99, G = 1{\cdot}02, H = 1{\cdot}06, I = 1{\cdot}09, J = 1{\cdot}13, K = 1{\cdot}17$. (*f*) Field modulus in perspective. (*g*) Wave fronts. The phase of the first and last fronts are respectively 0 and $12{\cdot}5 \times 2\pi$.

A sequence of 50 wavefronts is plotted on figure 5(*g*). The phase interval between two successive fronts is a fraction of 2π radians

$$\Delta\phi = 12{\cdot}5 \times 2\pi/49 = 0{\cdot}255(2\pi)$$

and slightly less than four fronts constitute a wavelength. The deformations observed in the central region are essentially caused by refraction, a faster propagation is apparent for $x_* > 0{\cdot}5$ and a retarded motion may be noticed for $x_* < 0{\cdot}5$.

Figures 6(*a–f*) give the results of a calculation performed for the same incident wavelength but a vortex with a radius $R_{M*} = 0{\cdot}0789$, double that of the previous case. The effect of refraction is stronger and induces larger mean phase and modulus variations.

Conclusion

The foregoing analysis clearly shows the utility of the parabolic equation method for the treatment of scattering of (acoustic) waves by various kinds of inhomogeneities. The parabolic equation may be solved numerically with efficient and precise finite

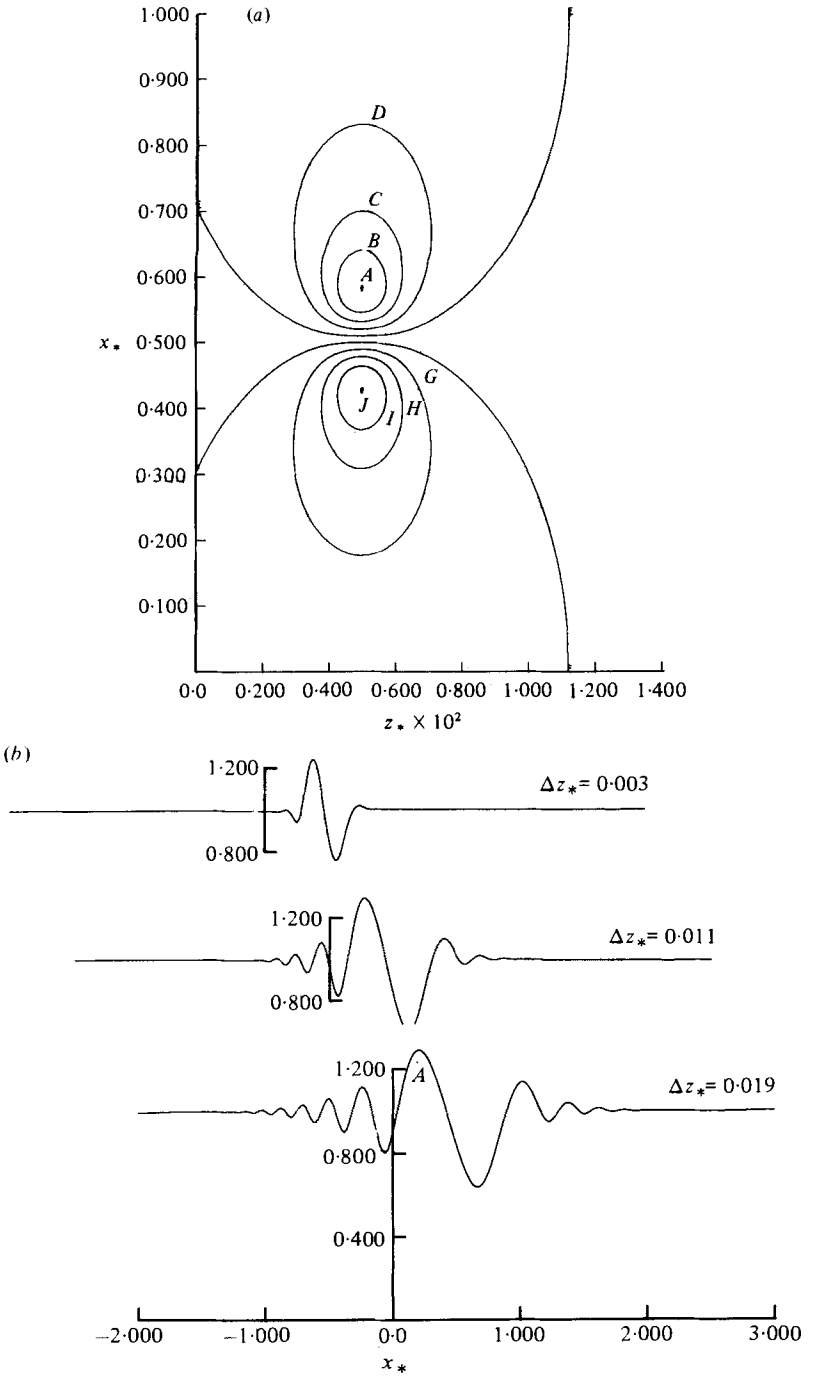

FIGURES 6 (*a*, *b*). For legend see page 498.

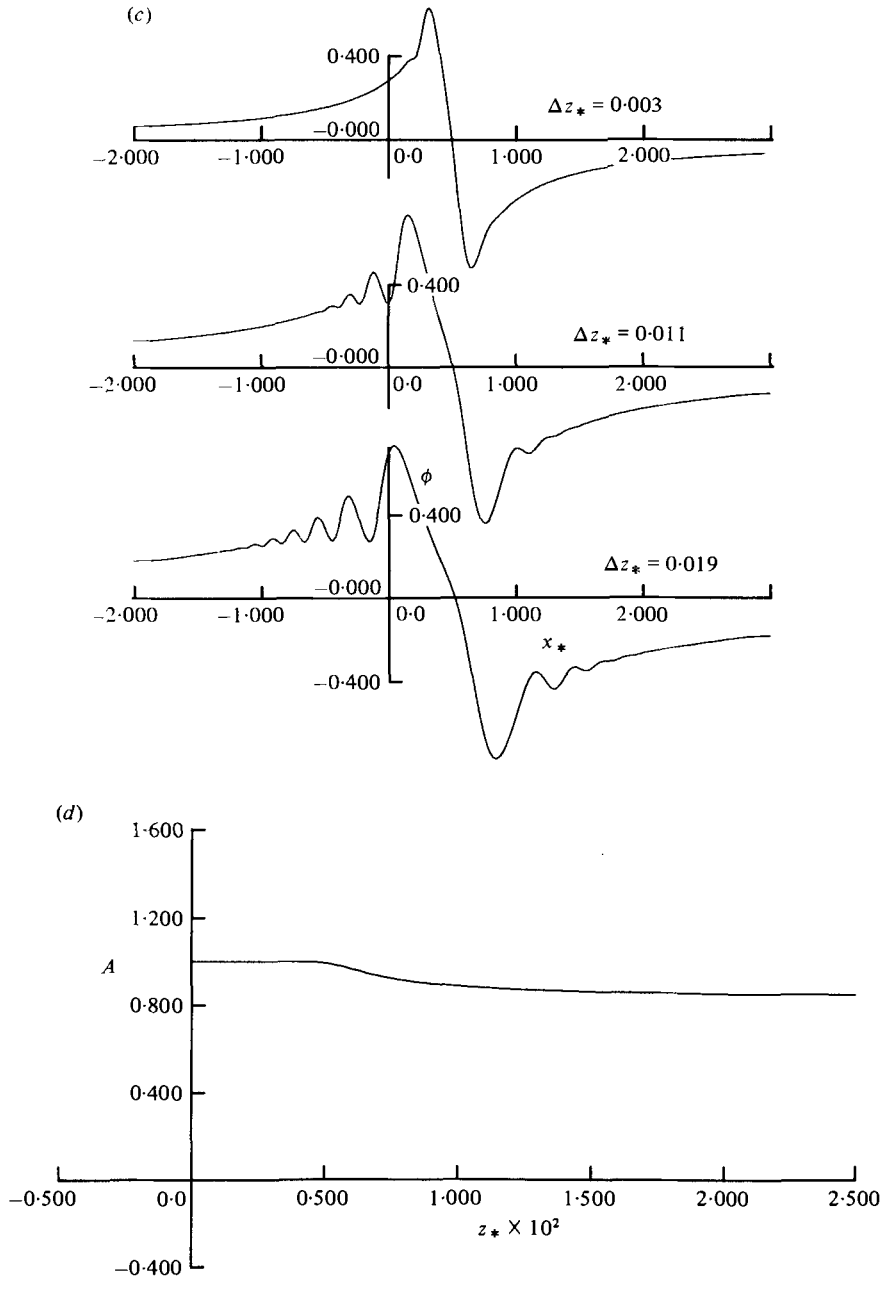

FIGURES 6(*c*, *d*). For legend see page 498.

difference methods and the results obtained in the simplest situations (circular and elliptical cylinder of uniform refraction index, viscous core vortex) are in qualitative (and sometimes quantitative) agreement with analytical solutions based on the Born approximation and interpreted according to the method of smooth perturbations. In all cases the parabolic approximation is superior to the more classical Born, smooth perturbation and geometrical approximations.

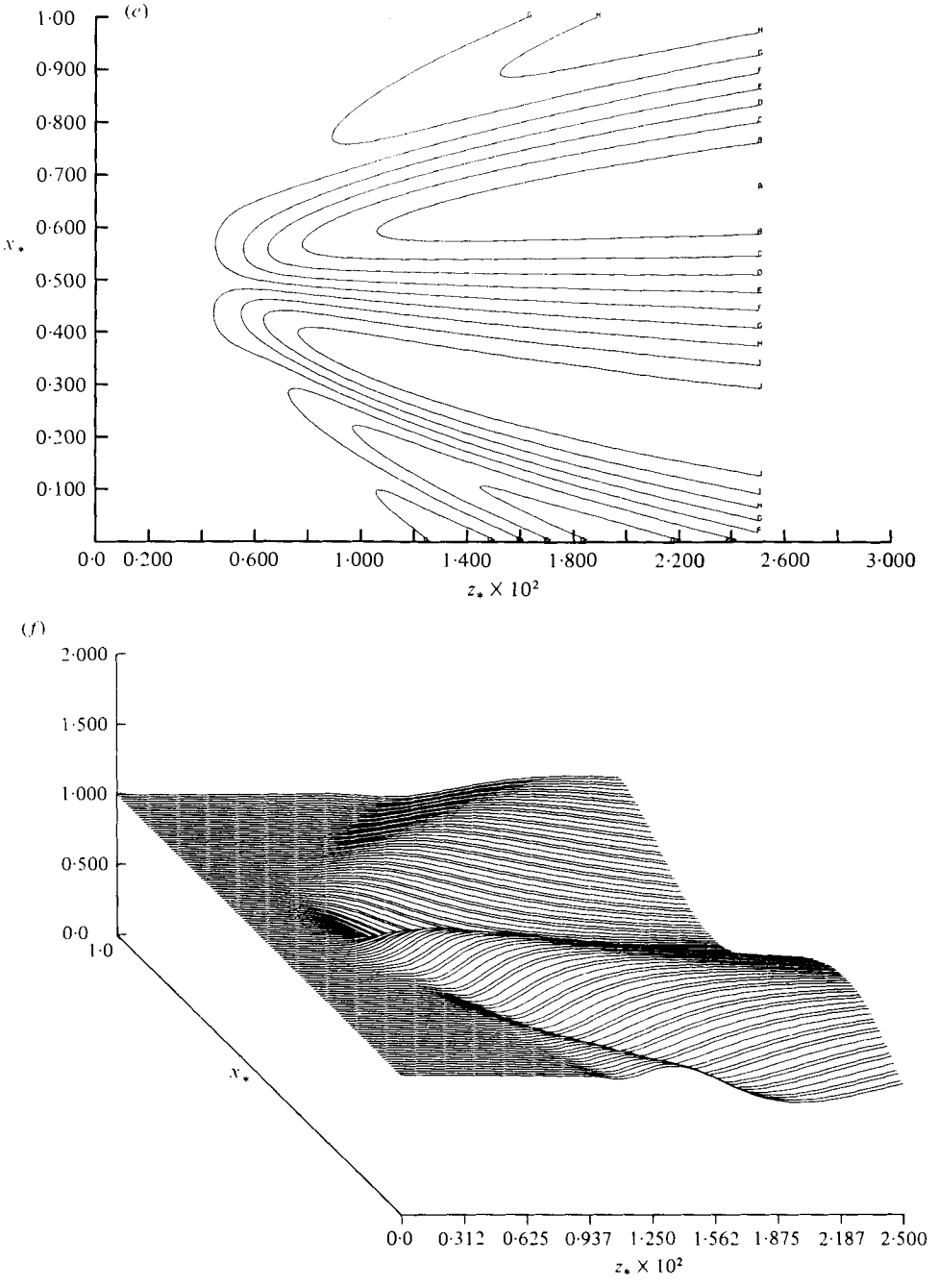

FIGURE 6. Scattering of a plane wave by a viscous core vortex. Conditions similar to those of figure 5 except that $R_{M*} = 0{\cdot}0779$. (*a*) Equivalent index plotted in iso-contour form $A = 0{\cdot}941$, $B = 0{\cdot}954$, $C = 0{\cdot}967$, $D = 0{\cdot}980$, $E = 0{\cdot}993$, $F = 1{\cdot}006$, $G = 1{\cdot}019$, $H = 1{\cdot}032$, $I = 1{\cdot}045$, $J = 1{\cdot}059$. (*b*) Field modulus in three axial sections $\bar{z}_* = 0{\cdot}003, 0{\cdot}011, 0{\cdot}019$. (*c*) Phase calculated with respect to the incident wave in three sections $\bar{z}_* = 0{\cdot}003, 0{\cdot}011, 0{\cdot}019$. (*d*) Variation of the field modulus on the $x_* = 0{\cdot}5$ axis. (*e*) Iso-contour plot of the field modulus $A = 0{\cdot}63$, $B = 0{\cdot}70$, $C = 0{\cdot}77$, $D = 0{\cdot}83$, $E = 0{\cdot}90$, $F = 0{\cdot}96$, $G = 1{\cdot}03$, $H = 1{\cdot}10$, $I = 1{\cdot}16$, $J = 1{\cdot}23$, $K = 1{\cdot}30$. (*f*) Field modulus in perspective.

The computer code used in this study was developed by the author at the Université de Technologie de Compiègne. All the results presented have been obtained during a summer visit to the California Institute of Technology made possible by Professor Frank Marble and a leave of absence authorized by ONERA. The author gratefully acknowledges various suggestions made by M. Robert Legendre (ONERA) and helpful discussions with Professors Frank Marble, Anatol Roshko, Edward Zukoski (CIT), John Laufer (USC), Pierre Alais (U. of Paris VI) and with Alain Julienne, Alain Guedel (ONERA) and Bernd Trebitz (CIT).

Appendix A. Scattering of a plane wave by a cylindrical inhomogeneity of circular section

This appendix presents the Born approximation analysis of the scattering of a plane wave by a circular cylinder inhomogeneity having a uniform refraction index. The solution of similar problems has been known for some time. Rayleigh (1881) and Gans (1925) treated the scattering of a plane wave by a diaphanous sphere (a description of this problem is also given in a textbook of Jones 1964, p. 513).

We seek a solution of the following inhomogeneous scalar wave equation

$$\nabla^2 p_s + k^2 p_s = -k^2(N^2-1)\,p_0, \tag{A 1}$$

where $p_0 = \exp(ik\mathbf{m}\,.\,\mathbf{r})$ represents the incident plane wave and p_s designates the scattered field. The two-dimensional Green's function

$$G(\mathbf{r}|\mathbf{r}_0) = \tfrac{1}{4}iH_0^1(k|\mathbf{r}-\mathbf{r}_0|), \tag{A 2}$$

may be used to write the solution of (A 1) in the form

$$p_s(\mathbf{r}) = \int k^2(N^2-1)\,p_0(\mathbf{r}_0)\,\tfrac{1}{4}iH_0^1(k|\mathbf{r}-\mathbf{r}_0|)\,d\mathbf{r}_0. \tag{A 3}$$

For a distant observation point that is for $k|\mathbf{r}-\mathbf{r}_0| \gg 1$ the Hankel function may be replaced by its asymptotic expansion

$$H_0^1 \sim \left(\frac{2}{\pi k|\mathbf{r}-\mathbf{r}_0|}\right)^{\frac{1}{2}} \exp(ik|\mathbf{r}-\mathbf{r}_0| - \tfrac{1}{4}i\pi). \tag{A 4}$$

If the observation point is in the far field of the scattering volume $r \gg r_0$, the previous expansion may be replaced by

$$H_0^1 \sim \left(\frac{2}{\pi kr}\right)^{\frac{1}{2}} \exp(ik|\mathbf{r}-\mathbf{r}_0| - \tfrac{1}{4}i\pi), \tag{A 5}$$

and the scattered field becomes

$$p_s(\mathbf{r}) \sim \tfrac{1}{4}\exp(\tfrac{1}{4}i\pi)\,k^2\left(\frac{2}{\pi kr}\right)^{\frac{1}{2}} \int (N^2-1)\,p_0(\mathbf{r}_0)\exp(ik|\mathbf{r}-\mathbf{r}_0|)\,d\mathbf{r}_0. \tag{A 6}$$

A classical (Fraunhofer) evaluation of expressions of this kind consists of replacing the distance $|\mathbf{r}-\mathbf{r}_0|$ by the first two terms of its power series expansion

$$|\mathbf{r}-\mathbf{r}_0| \simeq r - \mathbf{n}\,.\,\mathbf{r}_0, \quad \mathbf{n} = \mathbf{r}/r.$$

This yields

$$p_s(\mathbf{r}) = \frac{k^2\exp(\frac{1}{4}i\pi + ikr)}{2(2\pi kr)^{\frac{1}{2}}} \int (N^2-1)\exp(-ik(\mathbf{n}-\mathbf{m})\,.\,\mathbf{r}_0)\,d\mathbf{r}_0. \tag{A 7}$$

The scattered field appears as the Fourier transform of (N^2-1) with its argument equal to the converted wave vector $\mathbf{K} = k(\mathbf{n}-\mathbf{m})$. In the case of a uniform refraction index and a circular geometry it is convenient to evaluate (A 7) in polar co-ordinates:

$$\left.\begin{aligned} x_0 &= r_0\cos\theta, \quad z_0 = r_0\sin\theta, \\ K_x &= K\cos\phi, \quad K_z = K\sin\phi. \end{aligned}\right\} \tag{A 8}$$

Then

$$p_s(\mathbf{r}) = \frac{k^2\exp(\frac{1}{4}i\pi)}{2(2\pi kr)^{\frac{1}{2}}}\exp(ikr)(N^2-1)\int_0^{2\pi}d\theta\int_0^R \exp(-iKr_0\cos(\theta-\phi))\,r_0\,dr_0\,d\theta. \tag{A 9}$$

Using the classical integral representation of the zeroth-order Bessel function this expression becomes

$$p_s(\mathbf{r}) = k^2\exp(\tfrac{1}{4}i\pi+ikr)\left(\frac{\pi}{2kr}\right)^{\frac{1}{2}}(N^2-1)\int_0^R J_0(Kr_0)\,r_0\,dr_0, \tag{A 10}$$

which may be integrated by making use of another well-known identity

$$\frac{d}{d\zeta}[\zeta J_1(\zeta)] = \zeta J_0(\zeta). \tag{A 11}$$

The scattered field thus takes the final form

$$p_s(\mathbf{r}) = (kR)^2\left(\frac{\pi}{2kr}\right)^{\frac{1}{2}}(N^2-1)\frac{J_1(KR)}{KR}\exp(\tfrac{1}{4}i\pi+ikr), \tag{A 12}$$

where K designates the modulus of the converted wave vector $K = 2k|\sin\frac{1}{2}\Theta|$.

Appendix B. Scattering of a plane acoustic wave by a viscous core vortex

We analyse in this appendix the scattering of a plane acoustic wave by a viscous core vortex. The calculations, based on the Born approximation, resemble those of Ferziger (1974) and O'Shea (1975). However the computation techniques are somewhat simpler and our result differs slightly but significantly from those presented in the previous studies. We shall therefore present this development in some detail.

Equation (9) derived in § 2 provides a convenient starting point. In the absence of temperature fluctuations the scattered field is given by

$$\nabla^2 p_s + k^2 p_s = p_0\,2k^2\left(1-i\frac{\mathbf{m}\cdot\nabla}{k}\right)\frac{\mathbf{m}\cdot\mathbf{u}}{c_0}, \tag{B 1}$$

where the incident field is a plane wave propagating in the $\mathbf{m}$ direction:

$$p_0(\mathbf{r}) = A_0\exp(i\mathbf{k}\cdot\mathbf{r}) = A_0\exp(ik\mathbf{m}\cdot\mathbf{r}). \tag{B 2}$$

For a two-dimensional flow field the solution of this equation may be expressed in terms of the free space Green's function

$$G(\mathbf{r}|\mathbf{r}_0) = \tfrac{1}{4}iH_0^1(k|\mathbf{r}-\mathbf{r}_0|), \tag{B 3}$$

where H_0^1 the zeroth-order Hankel function behaves at infinity like a diverging cylindrical wave.

Then

$$p_s(\mathbf{r}) = \int -2k^2 \frac{\mathbf{m}.\mathbf{u}}{c_0} p_0(\mathbf{r}_0)\, \tfrac{1}{4}iH_0^1(k|\mathbf{r}-\mathbf{r}_0|)\, d\mathbf{r}_0 + \int \frac{2ik}{c_0} \mathbf{mm} : \nabla \mathbf{u} p_0(\mathbf{r}_0)\, \tfrac{1}{4}iH_0^1(k|\mathbf{r}-\mathbf{r}_0|)\, d\mathbf{r}_0. \tag{B 4}$$

An important simplification may be obtained by choosing the x_3 axis in the direction of incidence and the x_2 axis perpendicular to the flow field. Expression (B 4) thus becomes

$$p_s(\mathbf{r}) = \int -2k^2 \frac{u_3}{c_0} p_0(\mathbf{r}_0)\, \tfrac{1}{4}iH_0^1(k|\mathbf{r}-\mathbf{r}_0|)\, d\mathbf{r}_0 + \int \frac{2ik}{c_0} \frac{\partial u_3}{\partial x_3} p_0(\mathbf{r}_0)\, \tfrac{1}{4}iH_0^1(k|\mathbf{r}-\mathbf{r}_0|)\, d\mathbf{r}_0. \tag{B 5}$$

At this point it is necessary to use a far-field approximation and replace the Hankel function H_0^1 by its asymptotic form

$$H_0^1(k|\mathbf{r}-\mathbf{r}_0|) \sim \left(\frac{2}{\pi k|\mathbf{r}-\mathbf{r}_0|}\right)^{\frac{1}{2}} \exp\left(ik|\mathbf{r}-\mathbf{r}_0| - \tfrac{1}{4}i\pi\right). \tag{B 6}$$

This implies that the distance $|\mathbf{r}-\mathbf{r}_0|$ is large compared to the wavelength and in consequence the integration volume must be located sufficiently far from the observation point. However the velocity field under consideration behaving like r_0^{-1} is unbounded and using (B 6) is not rigorously justified. To overcome this difficulty we can limit the radius of the integration volume in a first step and then let this radius tend to infinity.

Now, an additional approximation is needed for evaluating (B 5). We use the classical Fraunhofer expansion and write (B 6) as

$$H_0^1(k|\mathbf{r}-\mathbf{r}_0|) \sim \left(\frac{2}{\pi kr}\right)^{\frac{1}{2}} \exp\left(ikr - ik\mathbf{n}.\mathbf{r}_0 - \tfrac{1}{4}i\pi\right), \tag{B 7}$$

where $\mathbf{n}$ designates the unit vector in the observation direction ($\mathbf{n} = \mathbf{r}/r$). The scattered field thus becomes

$$p_s(\mathbf{r}) = -\tfrac{1}{2}i\frac{k^2}{c_0}\left(\frac{2}{\pi kr}\right)^{\frac{1}{2}} \exp\left(ikr - \tfrac{1}{4}i\pi\right) A_0 \int u_3(\mathbf{r}_0) \exp\left(-ik(\mathbf{n}-\mathbf{m}).\mathbf{r}_0\right) d\mathbf{r}_0 - \frac{1}{2}\frac{k}{c_0}\left(\frac{2}{\pi kr}\right)^{\frac{1}{2}} \exp\left(ikr - \tfrac{1}{4}i\pi\right) A_0 \int \frac{\partial u_3}{\partial x_3}(\mathbf{r}_0) \exp\left(-ik(\mathbf{n}-\mathbf{m}).\mathbf{r}_0\right) d\mathbf{r}_0, \tag{B 8}$$

which may be written as

$$p_s(\mathbf{r}) = -\frac{A_0}{(2\pi kr)^{\frac{1}{2}}} \exp\left(ikr - \tfrac{1}{4}i\pi\right)\left(\frac{ik^2}{c_0} l_1 + \frac{k}{c_0} l_2\right), \tag{B 9}$$

where

$$l_1 = \int u_3(\mathbf{r}_0) \exp\left(-i\mathbf{K}.\mathbf{r}_0\right) d\mathbf{r}_0, \tag{B 10}$$

$$l_2 = \int \frac{\partial u_3}{\partial x_3}(\mathbf{r}_0) \exp\left(-i\mathbf{K}.\mathbf{r}_0\right) d\mathbf{r}_0, \tag{B 11}$$

$$\mathbf{K} = k(\mathbf{n}-\mathbf{m}).$$

l_1 and l_2 appear as the Fourier transforms of the axial velocity u_3 and its derivative in the x_3 direction. If these two expressions exist it is possible to write

$$l_2 = l_1 iK_3, \tag{B 12}$$

and the scattered field takes the general form

$$p_s(\mathbf{r}) = -\frac{A_0}{(2\pi kr)^{\frac{1}{2}}} \exp(ikr - \tfrac{1}{4}i\pi) \frac{ik^2}{c_0}\left(1+\frac{K_3}{k}\right) \int u_3(\mathbf{r}_0) \exp(-i\mathbf{K}.\mathbf{r}_0)\, d\mathbf{r}_0. \tag{B 13}$$

To calculate this field it is sufficient to evaluate the Fourier transform of u_3 for the converted wave vector $\mathbf{K}$. This feature is of great practical interest as multi-dimensional Fourier transforms may be efficiently determined with an FFT algorithm.

Now in the case of a viscous core vortex this numerical procedure is not necessary as (B 10) and (B 11) may be integrated analytically. The tangential velocity at a distance r from the vortex axis is

$$u_\theta(\mathbf{r}) = \frac{\Gamma}{2\pi r}(1-\exp(-r^2/R^2)). \tag{B 14}$$

If θ represents a polar angle measured from the x_1 axis the axial velocity is

$$u_3 = u_\theta(\mathbf{r})\cos\theta, \tag{B 15}$$

and the derivative of u_3 in the axial direction has the form

$$\frac{\partial u_3}{\partial x_3} = \tfrac{1}{2}\sin 2\theta\, r \frac{d}{dr}\left(\frac{u_\theta}{r}\right). \tag{B 16}$$

The converted wave vector $\mathbf{K}$ may be represented in polar co-ordinates by

$$K_1 = K\cos\phi, \quad K_3 = K\sin\phi,$$

and (B 10) and (B 11) become

$$l_1 = \int_0^\infty \int_0^{2\pi} u_\theta(\mathbf{r}_0)\cos\theta \exp(-iKr_0\cos(\theta-\phi))\, r_0\, dr_0\, d\theta, \tag{B 17}$$

$$l_2 = \int_0^\infty \int_0^{2\pi} r_0^2 \frac{d}{dr_0}\left(\frac{u_\theta}{r_0}\right) \tfrac{1}{2}\sin 2\theta \exp(-iKr_0\cos(\theta-\phi))\, dr_0\, d\theta. \tag{B 18}$$

We first consider l_1 and use the change of variable $\zeta = Kr_0$,

$$l_1 = \frac{1}{K^2}\int_0^\infty u_\theta\, \zeta\, d\zeta \int_0^{2\pi} \cos\theta \exp(-i\zeta\cos(\theta-\phi))\, d\theta. \tag{B 19}$$

The angular integral

$$L_1 = \int_0^{2\pi} \cos\theta \exp(-i\zeta\cos(\theta-\phi))\, d\theta, \tag{B 20}$$

becomes, after a few changes of variables,

$$L_1 = \cos\phi \int_{-\phi}^{2\pi-\phi} \exp(i(\theta - \zeta\cos\theta))\, d\theta, \tag{B 21}$$

and a formula given by Jones 1964, p. 70:†

$$J_n(\zeta) = \frac{1}{2\pi}\exp(\tfrac{1}{2}n\pi)\int_{\alpha}^{\alpha+2\pi}\exp(i(n\theta-\zeta\cos\theta))\,d\theta, \tag{B 22}$$

directly yields

$$L_1 = -i\cos\phi\, 2\pi J_1(\zeta). \tag{B 23}$$

Then expression (B 17) becomes

$$l_1 = \frac{\Gamma}{iK}\cos\phi\int_0^{\infty}(1-\exp(-\zeta^2/K^2R^2))\,J_1(\zeta)\,d\zeta. \tag{B 24}$$

Before completing this calculation we first write l_2 in a similar form. The change of variable $\zeta = Kr_0$ applied to (B 18) yields

$$l_2 = \frac{1}{K}\int_0^{\infty}\zeta^2\frac{d}{d\zeta}\left(\frac{u_\theta}{\zeta}\right)\int_0^{2\pi}\tfrac{1}{2}\sin 2\theta\exp(-i\zeta\cos(\theta-\phi))\,d\theta. \tag{B 25}$$

The integration over θ may be performed as before after a few changes of variables and an application of (B 22):

$$L_2 = \int_0^{2\pi}\sin 2\theta\exp(-i\zeta\cos(\theta-\phi))\,d\theta = -2\pi\sin 2\phi\, J_2(\zeta). \tag{B 26}$$

Substituting this result in expression (B 25) and integrating by parts leads to

$$l_2 = \Gamma\sin\phi\cos\phi\int_0^{\infty}(1-\exp(-\zeta^2/K^2R^2))\,J_1(\zeta)\,d\zeta. \tag{B 27}$$

Thus $l_2 = l_1\, iK\sin\phi = iK_3 l_1$, which is in agreement with expression (B 12).

To evaluate

$$L_3 = \int_0^{\infty}(1-\exp(-\zeta^2/K^2R^2))\,J_1(\zeta)\,d\zeta, \tag{B 28}$$

we let $a^2 = 1/K^2R^2$. L_3 is the difference of two integrals:

$$\int_0^{\infty}J_1(\zeta)\,d\zeta = 1, \tag{B 29}$$

and

$$\int_0^{\infty}\exp(-a^2\zeta^2)\,J_1(\zeta)\,d\zeta = \frac{\Gamma(1)}{4a^2\Gamma(2)}\,M\left(1,2,-\frac{1}{4a^2}\right). \tag{B 30}$$

The last expression is given by Abramovitz & Stegun (1965) (formula 11.4.28, p. 486) who also list (p. 509) the suitable hypergeometric function

$$M(1,2,2z) = \frac{e^z}{z}\sinh z. \tag{B 31}$$

Then

$$L_3 = \exp(-\tfrac{1}{4}K^2R^2), \tag{B 32}$$

† Watson (1962, p. 20), gives a different expression for $J_n(\zeta)$ which seems erroneous:

$$J_n(\zeta) = \frac{1}{2\pi}\int_{\alpha}^{\alpha+2\pi}\exp(i(n\theta-\zeta\cos\theta))\,d\theta.$$

and (B 24) and (B 27) become

$$l_1 = \frac{\Gamma}{iK}\cos\phi\exp(-\tfrac{1}{4}K^2R^2), \tag{B 33}$$

$$l_2 = \Gamma\sin\phi\cos\phi\exp(-\tfrac{1}{4}K^2R^2). \tag{B 34}$$

The scattered field is then obtained by inserting these expressions in (B 9):

$$p_s(\mathbf{r}) = -\frac{A_0}{(2\pi kr)^{\frac{1}{2}}}\exp(ikr-\tfrac{1}{4}i\pi)\frac{\Gamma k}{c_0}\exp(-\tfrac{1}{4}K^2R^2), \left[\frac{k}{K}\cos\phi+\sin\phi\cos\phi\right]. \tag{B 35}$$

This result is more convenient when written in terms of the scattering angle Θ. This transcription may be performed with

$$\begin{aligned} K &= 2k|\sin\tfrac{1}{2}\Theta|,\\ K\cos\phi &= k(\mathbf{n}-\mathbf{m})_1 = -k\sin\Theta,\\ K\sin\phi &= k(\mathbf{n}-\mathbf{m})_3 = k(\cos\Theta-1), \end{aligned} \tag{B 36}$$

and the scattered field finally becomes

$$p_s(\mathbf{r}) = \frac{A_0}{(2\pi kr)^{\frac{1}{2}}}\exp(ikr-\tfrac{1}{4}i\pi)\frac{\Gamma k}{c_0}\exp(-\tfrac{1}{4}K^2R^2), [\tfrac{1}{2}\cot\tfrac{1}{2}\Theta-\sin\tfrac{1}{2}\Theta\cos\tfrac{1}{2}\Theta]. \tag{B 37}$$

This expression may be compared to that obtained by O'Shea (1975) (expression 37), which in our notations appears as

$$p_s(\mathbf{r}) = -\frac{1}{2\pi}\frac{A_0}{(2\pi kr)^{\frac{1}{2}}}\exp(ikr-\tfrac{1}{4}i\pi)\frac{\Gamma k}{c_0}\quad[\tfrac{1}{2}\cot\tfrac{1}{2}\Theta+\sin\tfrac{1}{2}\Theta\cos\tfrac{1}{2}\Theta]. \tag{B 38}$$

One notes the absence of $\exp(-\frac{1}{4}K^2R^2)$, the presence of an additional $(2\pi)^{-1}$ factor and a difference in sign.

Turning now to the scattered field given by Ferziger (1974) (his expression A 7)† we note that it has incorrect dimensions and misses a factor $(2\pi kr)^{-\frac{1}{2}}$. Correcting these deficiencies and performing the remaining integration leads us to

$$p_s(\mathbf{r}) = \frac{1}{2\pi}A\frac{\Gamma k}{c_0}\frac{\exp(ikr)}{(2\pi kr)^{\frac{1}{2}}}[|\sin\tfrac{1}{2}\Theta|\cos\tfrac{1}{2}\Theta-\tfrac{1}{2}\cot\tfrac{1}{2}\Theta]\exp(-\tfrac{1}{4}K^2R^2). \tag{B 39}$$

The term in the bracket appears in the same form as that of (B 37) but its sign does not change with Θ. In addition we note the presence of a $(2\pi)^{-1}$ factor and the absence of $\exp(-\frac{1}{4}i\pi)$.

Finally it is worth calculating the scattering cross-section using the scattered field (B 37). This 'cross-section' may be defined by the ratio

$$\sigma(\Theta) = \frac{p_s^2(\Theta)\,2\pi r/\rho_0 c}{p_0^2/\rho_0 c} \tag{B 40}$$

† $p_s = \dfrac{Ak}{\omega}\exp(ikr)(\sin\theta\sin\tfrac{1}{2}\theta-\cos\tfrac{1}{2}\theta)\int r'dr'J_1(kr')\,u_\theta(r')$.

and in cylindrical geometry it has the dimension of a length:

$$\sigma(\Theta) = \frac{1}{4}\left(\frac{\Gamma}{c_0}\right)^2 k \exp\left(-\tfrac{1}{2}K^2R^2\right)\cos^2\Theta\cot^2\tfrac{1}{2}\Theta. \tag{B 41}$$

Appendix C. Relation between the method of smooth perturbation and the Born approximation

Consider the following equation:

$$\nabla^2 p + k^2N^2 p = 0. \tag{C 1}$$

The solution of this equation may be sought in the form of a Neumann series

$$p = p_0 + p_1 + p_2 + \ldots, \tag{C 2}$$

where the successive terms are given by

$$\left.\begin{aligned} &\nabla^2 p_0 + k^2 p_0 = 0, \\ &\nabla^2 p_1 + k^2 p_1 = -k^2(N^2-1)\,p_0, \\ &\nabla^2 p_2 + k^2 p_2 = -k^2(N^2-1)\,p_1. \end{aligned}\right\} \tag{C 3}$$

The zeroth-order term represents the incident wave. The first-order term is the scattered field in the so-called Born approximation

$$p_1(\mathbf{r}) = \int k^2(N^2-1)\,p_0(\mathbf{r}_0)\,G(\mathbf{r}|\mathbf{r}_0)\,d\mathbf{r}_0, \tag{C 4}$$

where $G(\mathbf{r}|\mathbf{r}_0)$ designates the free space Green's function for the Helmholtz equation.

In the method of smooth perturbation (Tatarski 1961) the field is sought in the form

$$p(\mathbf{r}) = \exp(\phi(\mathbf{r})), \tag{C 5}$$

and (C 1) is replaced by

$$\nabla^2\phi + (\nabla\phi)^2 + k^2N^2 = 0.$$

Instead of the Neumann expansion (C 2), ϕ is written as a series

$$\phi = \phi_0 + \phi_1 + \phi_2 + \ldots, \tag{C 6}$$

where the successive terms satisfy the following equations:

$$\left.\begin{aligned} &\nabla^2\phi_0 + (\nabla\phi_0)^2 + k^2 = 0, \\ &\nabla^2\phi_1 + 2\nabla\phi_0 \cdot \nabla\phi_1 = -k^2(N^2-1), \\ &\nabla^2\phi_2 + 2\nabla\phi_0 \cdot \nabla\phi_2 = -(\nabla\phi_1)^2, \\ &\ldots. \end{aligned}\right\} \tag{C 7}$$

The solution of the first equation is $\phi_0 = \ln p_0$.

The second equation may be solved by writing ϕ_1 in the form

$$\phi_1 = \exp(-\phi_0(\mathbf{r}))\,w(\mathbf{r}). \tag{C 8}$$

This yields for w

$$\nabla^2 w + k^2 w = -k^2(N^2-1)\exp(\phi_0), \tag{C 9}$$

so that

$$w(\mathbf{r}) = \int k^2(N^2-1)\exp(\phi_0(\mathbf{r}_0))\,G(\mathbf{r}|\mathbf{r}_0)\,d\mathbf{r}_0. \tag{C 10}$$

Then the first-order term in the series expansion of ϕ becomes

$$\phi_1(\mathbf{r}) = \frac{1}{p_0(\mathbf{r})}\int k^2(N^2-1)\,p_0(\mathbf{r}_0)\,G(\mathbf{r}|\mathbf{r}_0)\,d\mathbf{r}_0. \tag{C 11}$$

A comparison of expressions (C 4) and (C 11) leads to the following identity:

$$\phi_1(\mathbf{r}) = p_1(\mathbf{r})/p_0(\mathbf{r}). \tag{C 12}$$

If the higher-order terms in the series of ϕ are negligible, the real part of ϕ_1 represents the logarithmic amplitude of the sound field and its imaginary part provides the phase of the field with respect to the incident wave p_0. Indeed

$$p_0 = A_0 \exp(i\phi_0), \tag{C 13}$$

$$p = A\exp(i\phi) = A_0\exp(i\phi_0+\phi_1), \tag{C 14}$$

and

$$\ln A/A_0 = \mathrm{Re}\,(\phi_1) = \mathrm{Re}\,(p_1/p_0), \tag{C 15}$$

$$\phi-\phi_0 = \mathrm{Im}\,(\phi_1) = \mathrm{Im}\,(p_1/p_0). \tag{C 16}$$

In conclusion the solution of problem (C 1) in the framework of the method of smooth perturbation to the first order may be obtained by seeking the Born approximation solution of the same problem and then interpreting the result with the last two expressions.

REFERENCES

Abramovitz, M. & Stegun, I. A. 1965 *Handbook of Mathematical Functions*. Dover.

Baerg, W. & Schwarz, W. H. 1966 Measurement of the scattering of sound from the turbulence. *J. Acoust. Soc. Am.* **39**, 1125.

Barabanenkov, Yu. N., Kravtsov, Yu. A., Rytov, S. M. & Tatarski, V. I. 1971 Status of the theory of propagation of waves in a randomly inhomogeneous medium. *Sov. Phys.* **13**, 551.

Brown, G. & Roshko, A. 1974 On density effect and large structure in turbulent mixing layers. *J. Fluid Mech.* **64**, 775.

Butler, G. F., Holbeche, T. A. & Fethney, P. 1973 Some experimental observations of the refraction of sound by a rotating flow. *AGARD Conf. Proc.* no. 131, p. 91.

Candel, S. M. 1976 Application of geometrical techniques to aeroacoustic problems. *A.I.A.A. Paper* no. 76-546.

Candel, S. M. 1977 Résolution numérique de problèmes de propagation et de rayonnement à l'aide de l'approximation parabolique. *Univ. Tech. Compiègne Tech. Rep.* no. 5–1978.

Candel, S. M., Guédel, A. & Julienne, A. 1975 Refraction and scattering in an open wind tunnel flow. *Proc. 6th Int. Cong. Instrumentation in Aerospace Simulation Facilities, Ottawa*, p. 288.

Candel, S. M., Guédel, A. & Julienne, A. 1976*a* Résultats préliminaires sur la diffusion d'une onde acoustique par un écoulement turbulent. *Cong. Soc. Française Phys. Dijon* 1975. *J. de Physique* **37**, C1–153.

Candel, S. M., Guédel, A. & Julienne, A. 1976*b* Radiation refraction and scattering of acoustic waves in a free shear flow. *A.I.A.A. Paper* no. 76-544.

Candel, S. M., Guédel, A. & Julienne, A. 1977 Diffusion d'une onde monochromatique par un écoulement turbulent. *Euromech* 94: *Propagation des Ondes dans les Milieux Inhomogènes, Marseille.*

Candel, S. M., Julienne, A. & Julliand, M. 1976 Shielding and scattering by a jet flow. *A.I.A.A. Paper* no. 76-545.

Claerbout, J. F. 1976 *Fundamentals of Geophysical Data Processing*. McGraw-Hill.

Clifford, S. F. 1972 Propagation and scattering in random media. In *Remote Sensing of the Troposphere* (ed. V. E. Derr). University of Colorado, Boulder.

CLIFFORD, S. F. & BROWN, E. H. 1970 Propagation of sound in a turbulent atmosphere. *J. Acoust. Soc. Am.* **48**, 1123.

DE SANTO, J. A., PERKINS, J. S. & BAER, J. N. 1977 Corrections to the parabolic equation for sound propagation modelling. *J. Acoust. Soc. Am.* **61**, S 12(A).

DOWDLING, A. P. 1975 The refraction of sound by a shear layer made up of discrete vortices. *Aero. Res. Counc. R. & M.* no. 3770.

FERZIGER, J. H. 1974 Low frequency acoustic scattering from a trailing vortex. *J. Acoust. Soc. Am.* **56**, 1705.

FFOWCS WILLIAMS, J. E. & HOWE, M. S. 1973 On the possibility of turbulent thickening of weak shock waves. *J. Fluid Mech.* **58**, 461.

FRISCH, U. 1968 Wave propagation in random media. In *Probabilistic Methods in Applied Mathematics*, vol. 1 (ed. A. T. Barucha Reid). Academic Press.

GANS, R. 1925 *Ann. Phys.* **76**, 29.

GEORGES, T. M. 1972 Acoustic ray paths through a model vortex. *J. Acoust. Soc. Am.* **51**, 206.

HARDIN, R. H. & TAPPERT, F. D. 1973 Application of the split step Fourier method to the numerical solution of nonlinear and variable coefficient wave equations. *SIAM Rev.* **15**, 423.

HOWE, M. S. 1973 Multiple scattering of sound by turbulence and other inhomogeneities. *J. Sound Vib.* **27**, 455.

HUANG, M. N. 1975 Sound scattering from atmospheric turbulence. *A.I.A.A. Paper* no. 75-544.

ISHIMARU, A. 1977 Theory and application of wave propagation and scattering in random media. *Proc. I.E.E.E.* **65**, 1030.

JONES, D. S. 1964 *The Theory of Electromagnetism*. Pergamon.

KELLEY, P. L. 1965 Self focusing of optical beams. *Phys. Rev. Lett.* **15**, 1005.

LAU, J. C. & FISHER, M. J. 1975 The vortex sheet structure of turbulent jets. Part 1. *J. Fluid Mech.* **67**, 299.

LEGENDRE, R. 1968 Interprétation des mesures de turbulence. *ONERA Tech. Note* no. 138.

LIGHTHILL, M. J. 1953 On energy scattered from the interaction of turbulence with sound or shock waves. *Proc. Camb. Phil. Soc.* **49**, 531.

LILLY, J. Q. & MILLER, T. G. 1977 Target intensity enhancement for repetitively pulsed laser beams. *A.I.A.A. J.* **15**, 434.

MCDANIEL, S. T. 1975 Propagation of normal mode in the parabolic approximation. *J. Acoust. Soc. Am.* **57**, 307.

MCDANIEL, S. T. 1976 *J. Acoust. Soc. Am.* **58**, 1178.

MONIN, A. S. 1962 Characteristics of the scattering of sound in a turbulent atmosphere. *Sov. Phys. Acoust.* **7**, 370.

MULLER, E. A. & MATSCHAT, K. R. 1959 The scattering of sound by a single vortex and by turbulence. Max-Planck-Institut für Strömungsforschung Technical Report, Göttingen.

O'SHEA, S. 1975 Sound scattering by a potential vortex. *J. Sound Vib.* **43**, 109.

RAYLEIGH, LORD 1881 *Phil. Mag.* **12**, 81.

ROSHKO, A. 1976 Structure of turbulent shear flows: a new look. *A.I.A.A. J.* **14**, 1349.

TATARSKI, V. I. 1961 *Wave Propagation in a Turbulent Medium*. Dover.

TATARSKI, V. I. 1971 *The Effects of the Turbulent Atmosphere on Wave Propagation*. Israel Program of Scientific Translations, Jerusalem.

ULRICH, P. B. 1975 Numerical methods in high power laser propagation. In *Optical Propagation in the Atmosphere. AGARD Conf. Proc.* no. 183.

WALLACE, J. & LILLY, J. Q. 1974 Thermal blooming of repetitively pulsed laser beams. *J. Opt. Soc. Am.* **64**, 1651.

WATSON, G. N. 1962 *Theory of Bessel functions*, 2nd edn. Cambridge University Press.

WINANT, C. D. & BROWAND, F. K. 1974 Vortex pairing: the mechanism of turbulent mixing layer growth at moderate Reynolds numbers. *J. Fluid Mech.* **61**, 237.

WOUDE, P. V. D. & BREMMER, H. 1975 Expansions applicable to a non-stationary scattering medium. *Radio Sci.* **10**, 23.